The Contribution of Motility and Chemotaxis in the *Borrelia burgdorferi* infectious life cycle

by

Aaron Yerke

August, 2013

Director of Thesis: M.D. Motaleb

Major Department: Biomedical Sciences

Lyme disease has emerged as an increasing problem for people in the east and northeastern part of the United States. It can cause a chronic debilitating infection if left untreated and is difficult to diagnose. The illness is caused by an infection with the spirochete known as *Borrelia burgdorferi. B. burgdorferi* is a Gram-negative bacterium that is transmitted by ticks of the *Ixodes* genus. The primary carriers in regions of high Lyme disease incidence are *Ixodes scapularis* vector and white-footed *Mus musculus* rodents. *B. burgdorferi* is not known to produce common virulence factors such as toxins or capsules. Chemotaxis and motility are important for *B. burgdorferi* to cause infection and are considered as invasive attributes of this organism. Only a handful of studies have reported that non-chemotactic and non-motile *B. burgdorferi* mutants are unable to disseminate in hosts, and are, therefore, non-infectious in mice. Although motility and chemotaxis has been shown to be crucial for the infectious life cycle of *B. burgdorferi*, little is known about the mechanism of motility or assembly of periplasmic flagella. It is not known how incremental reductions of motility affect *B. burgdorferi*'s virulence. Recent cryo-electron microscopy tomography revealed that spirochetes possess a unique flagellar structure called the collar. However, the gene or genes that encode for the *B. burgdorferi* collar proteins are unknown. Because of its location in the periplasmic

flagellar motor, we hypothesize that this organelle is important for flagellar assembly as well as motility. We also hypothesize that less motile or less chemotactic mutants will exhibit a reduced invasive phenotype *in vivo*. Using Bioinformatics techniques, two potential candidate genes were identified (*bb0526* and *bb0773*) that may encode the collar. These two genes are annotated as putative genes in the *B. burgdorferi* genome with no significant similarity to other bacterial species outside of spirochetes. A BLAST search indicated that *bb0526* has homology to an unconfirmed motility gene in *Treponema pallidum*, another spirochete. A third gene, *fliZ*, putatively encodes a regulator of the flagella assembly complex. In other bacteria, inactivation of *fliZ* creates a reduced motile phenotype. Two genes that are hypothesized to have chemotactic function are *cheY1* and *cheY2*. Inactivation of these genes creates mutants with a phenotype indistinguishable from wild type *in vitro*. However, they may exhibit a different phenotype *in vivo*. In order to test our hypotheses, mutants for *cheY1*, *cheY2, bb0526, bb0773,* and *fliZ* were created. Our results show that the Δ*bb0773* mutant exhibits no discernible defects with respect to motility or morphology; the Δ*bb0526* mutant is associated with the collar structure and has a decreased motility defect. Inactivation of *fliZ* creates a mutant with a reduced number of periplasmic flagella and the wild type phenotype is restored upon complementation *in trans*. To demonstrate if reduced motility or chemotaxis is important for survivability or transmission between hosts, we plan to assay these mutants in mouse-tick-mouse infection cycle experiments.

The Contribution of Motility and Chemotaxis in the *Borrelia burgdorferi* infectious life cycle

A Thesis

Presented To the Faculty of the Biomedical Sciences Program

East Carolina University

In Partial Fulfillment Of the Requirements for the Degree

Master of Science in Biomedical Sciences

By:

Aaron Yerke

August 2013

Contribution of Motility and Chemotaxis in *Borrelia burgdorferi* Infectious Life Cycle

Presented To the Faculty of the Biomedical Sciences Program

by

Aaron Yerke

APPROVED BY:

DIRECTOR OF
DISSERTATION/THESIS: _____
MD Motaleb, PhD

COMMITTEE MEMBER: _____
C. Jeffery Smith, PhD

COMMITTEE MEMBER: _____
Daniel Martin, PhD

COMMITTEE MEMBER: _____
Mary Farwell, PhD

PROGRAM DIRECTOR OF
BIOMDICAL SCIENCE PROGRAM: _____
Rich Franklin, PhD

DEAN OF THE
GRADUATE SCHOOL: _____
Paul J. Gemperline, PhD

Acknowledgements

First and foremost I offer my sincerest gratitude to my advisor, Dr. Md. Motaleb, who has supported me throughout my work on thesis with his patience and knowledge. It is due to his guidance and effort that my thesis was able to be written. One simply could not wish for a more patient or friendlier advisor.

Without Drs Xiaowei Zhao and Jun Liu from the University of Texas at Houston this manuscript would be woefully incomplete, as they provided all of the Cryo-ET data and images. A special thanks to them. Additionally, I would like to thank my committee members, Drs. Mary Farwell, Daniel Martin, and C. Jeffrey Smith, taking the time to work with me and helping me to graduate on time.

I owe a great deal to my teammates in the Motaleb laboratory. Everyone in the lab has helped me and I would not have been able to complete my work without them. I want to thank Akarsh Manne for my initial training, whose expertise was always available if I needed it. Dr. Syed Sultan was always ready to lend a hand with an experiment or to provide advice if needed, and whose cheerful demeanor helped to make bench work more enjoyable. I want to especially thank Dr. Liz Novak for reviewing countless drafts of my thesis, as her help was invaluable for its completion. I want to thank Ki Hwan Moon for being a positive role-model and a fantastic roommate, who was always ready to help in or out of the laboratory. I would like to thank Kate Lees for her exuberance and friendly atmosphere.

I appreciate and thank the Biotech students and staff for providing a great learning environment. Lastly, I would like to thank my parents for their encouragement and support.

TABLE OF CONTENTS

LIST OF TABLES

LIST OF FIGURES

CHAPTER 1: INTRODUCTION

1.1 Lyme disease

Lyme disease owes its name to Lyme and Old Lyme, two towns in Connecticut where doctors documented that children were developing juvenile rheumatoid arthritis in the early 1970's (1). This arthritis was quickly recognized to be an epidemic problem as many more cases were reported in the mid-1970s, and not just by children, but adults as well (2, 3). Accompanying the arthritis were a medley of symptoms, including fever, fatigue, headache, myalgia, and skin rash (2). The disease that was described in Lyme was found to be prevalent throughout eastern and northeastern United States, and the incidence of this disease was cyclic (3). One of the most noticeable symptoms of this disease was a bull's eye shaped rash known as *Erythema chronicum migrans* (3). Such a rash had previously been seen in Europe as the result of the bite of a tick known as *Ixodes ricinus*, thus, indicating that the Lyme disease may be similarly transmitted by ticks in the United States (3).

In 1982, Willy Burgdorfer published his discovery of an *Ixodes scapularis* tick that was infected with a previously unknown spirochete of the *Borrelia* family. Bites from infected ticks caused lesions in rabbits, and the spirochete reacted with serum of Lyme disease patients (4). It was subsequently shown that this spirochete was the causative agent of Lyme disease and it was named *Borrelia burgdorferi* after its discoverer (5).

The cyclic nature of Lyme disease is due to the fact that it is a zoonotic illness. In nature, *B. burgdorferi* resides in two disparate hosts, *Ixodes* ticks and small rodents (5). Because of the zoonotic cycle, the rate of Lyme disease fluctuates throughout the year. However, it is the most commonly reported vector-borne illness in the United States. The cases of Lyme disease have increased considerably since 1992 (6) and it is now considered an emerging infectious

disease. In 2011, there were 24,364 confirmed and 8,733 probable cases of Lyme disease in the United States according to the Centers for Disease Control and Prevention (CDC) (7).

B. burgdorferi is a Gram-negative spirochete and an obligate microaerophilic anaerobe (8). It has a flat-wave morphology and ranges from 4 to 30 µm in length and has a diameter of approximately 0.3 µm (5). As with other spirochetes, *B. burgdorferi* has two membrane layers, the inner and the outer membranes. In between the outer membrane and peptidoglycan layer is the periplasmic space. In this space, the flagella of *B. burgdorferi* are located. The unique flat-wave morphology is due to the wrapping of these active flagella around the protoplasmic cell cylinder created by the inner membrane (5).

B31 was the first strain of *B. burgdorferi* to be isolated and sequenced (5). The genome of *B. burgdorferi* is unique in several ways. First and foremost of these is that in addition to a large linear 910 kb chromosome, *B. burgdorferi* possesses 21 extrachromosomal DNA elements with 12 linear and 9 circular plasmids, the most endogenous genetic elements of any bacterial genomes sequenced to-date. The convention for naming these plasmids is to indicate if it is circular (cp) or linear (lp) and then the length of the plasmid in kilo base pairs. For example, lp25 is a linear plasmid 25 kb in length. If there are more than one of a given type and size of plasmid, they are numbered, such as lp28-1. The extrachromosomal elements add an additional 611 kb of genomic material. In a laboratory setting, there are 11 plasmids that are dispensable and *B. burgdorferi* will survive in artificial media without them. Six of these, cp9, cp32–3, lp21, lp28–2, lp28–4, and lp56, are also dispensable for growth *in vivo* (9). Two plasmids, lp56 and lp25, harbor restriction modification enzymes, thus their presence creates challenges for genetic modification (10). Several plasmids, such as lp28-1 and lp25, are required for infection and persistence in the host and their loss during cultivation *in vitro* attenuates the bacteria (11).

Another uncommon feature of bacterial genomes is pseudogenes –*B. burgdorferi* has 167 such genes (12).

The optimal growth conditions for *B. burgdorferi* are 34°C to 37°C in a 2-3% CO_2 humidified incubator. *B. burgdorferi* is a relatively slow-growing bacterium with a doubling time of 5 to 12 hours at optimal conditions (5). The organism's relatively small genome size indicates that *B. burgdorferi* lacks many metabolic pathways and therefore it is considered as a fastidious bacterium and must be grown *in vitro* in complex, nutrient rich "Barbour-Stoenner-Kelly II" media (BSK-II). The constituents of this media are: CMRL 1066, neopeptone, bovine serum albumin (Fraction V), yeastolate, N-2-hydroxyethylpiperazine, N-2-ethanesulfonic acid, glucose, sodium citrate, sodium pyruvate, N-acetylglucosamine, sodium bicarbonate, and rabbit serum (13). It was designed to emulate *B. burgdorferi*'s natural tick and mammalian host environments (13).

B. burgdorferi is a highly mobile and invasive pathogen (14). Genome sequence analysis suggests that *B. burgdorferi* lacks common virulence factors such as toxins or lipopolysaccharide but contains large numbers of lipoproteins (6-7% of total genome) that induce host inflammation (15). Despite formidable challenge in genetic manipulations, recent reports indicate that *B. burgdorferi* virulence factors that contributed to either infection in experimental mice or survivability in ticks, or both, are: complement inhibition, decorin, fibronectin, plasminogen, laminin and integrin binding proteins, outer surface proteins (e.g., OspA, OspB, and OspC), VlsE which undergoes antigenic variations during mammalian infection, c-di-GMP metabolizing proteins, and many more (16). Moreover, although only a few studies have been reported, their results indicate that chemotaxis and motility are important for infection as well as transmission from ticks to naïve mice (17-19).

Since its discovery, much has been learned about the progression of Lyme disease. There are three stages of a *B. burgdorferi* infection, but it is possible to have symptoms of any stage out of order (20). Because of the lack of definite progression and vague symptoms, misdiagnosis is common (21).

Stage I is the first stage in a Lyme disease infection (20). Patients with a stage I infection have a wide range of symptoms such as malaise, fatigue, headache, fever, chills, stiff neck, arthralgias, myalgias, lymphadenopathy, and other less common symptoms (22). Stage I can last for weeks after the initial *B. burgdorferi* infected tick bite and is said to be over when the symptoms become more severe (20). In 70-80 percent of the cases, *Erythema chronicum migrans* presents 2 to 32 days after infection, making it a good clinical indicator of infection (22). Often the *Erythema migrans* shows a 'bull's eye pattern around the tick bite site, but the rash can show up anywhere and it can vary in shape, size, and location (23). The rash is caused by peripheral lymphocytic and eosinophilic infiltration of cutaneous vessels as they attempt to contain the *Borrelial* infection (24, 25). Lyme disease patients that go untreated can have a recurrence of *Erythema migrans* 1 to 14 months later (20).

As the spirochetes disperse through the body tissue, weeks or months after the initial tick bite, stage II infections are said to start (20). Neurological symptoms such as meningoradiculitis, which is inflammation of the meninges and the cranial or spinal nerve roots, can occur resulting in peripheral and central nervous dysfunction due to lymphocytic infiltration. Some of the major manifestations of the neural symptoms are insomnia, photophobia, and facial palsy (22). Some patients also develop new cutaneous symptoms at this point (20). At this stage, Lyme carditis is also possible (20). This carditis manifests most often as atrioventricular blockage due to inflammation, the presence of the spirochete, or both (26).

Stage III of Lyme disease starts six months after the initial tick bite. This is based on time alone, and not symptoms (20). The neurological symptoms become more severe, as do the skin and cardiac conditions. The skin begins to atrophy, with a condition called acrodermatitis chronica atrophicans of Herxheimer (20). Cardiac problems develop in approximately one percent of patients, but can lead to death (27).

A common symptom at this point is Lyme arthritis, which is characterized by asymmetric swelling of a joint, sometimes accompanied by pain. Lyme arthritis comes in two forms: intermittent arthritis, which is characterized by spells of arthritis followed by arthritis-free periods, and chronic arthritis, which lacks the arthritis-free periods. The CDC reports that 33 percent of all Lyme disease patients report arthritis (7). When untreated by antibiotics, 62 percent of patients of one study developed Lyme arthritis (28). The most common site of Lyme arthritis is the knees, followed by the shoulder and back (28).

Antibiotic refractory patients continue to exhibit symptoms even after a seemingly successful treatment of antibiotics. In one study, children with Lyme arthritis were treated with antibiotics and 23% of those children became antibiotic refractory (29). The antibiotic refractory Lyme arthritis may be caused by infection-induced autoimmunity, retained spirochete antigens, or both. This has led researchers to search for another mechanism to cause the symptoms, such as molecular mimicry. OspA, a *B. burgdorferi* outer-surface protein, shares an epitope (amino acids 163-175) with the human histocompatibility leukocyte antigen (hHCL) DR4-A. The hHCL DR4-A is used by the immune system to recognize cells as ‘self’ (30). It is possible that antibodies against OspA are reacting with hHCL DR4-A, causing the inflammation that results in Lyme arthritis (30).

There are many antibiotics that can cure stage I and stage II Lyme disease. For example, treatment of tetracycline over a period of 10 days cures Lyme disease quite well (31). Currently, there is no vaccine available for Lyme disease. A vaccine against recombinant OspA was pulled from the market for humans in 2002 due to low demand (32). OspA is an outer membrane surface protein that is up-regulated when *B. burgdorferi* is in the tick midgut, and then down-regulated when the tick begins feeding (33) . A similar vaccine, but using OspA and OspB, is available for dogs. OspB is also up-regulated when *B. burgdorferi* is in the midgut of the tick (34).

1. 2 The *Ixodes* family of ticks

It is through the bite of the *Ixodes* family of ticks that *B. burgdorferi* transmits between arthropod and vertebrate hosts (rodents are the primary reservoir). *B. burgdorferi* is an obligate pathogen (35). The vertebrate hosts are generally thought to be mammals, but birds, and even lizards can be hosts for *B. burgdorferi* (36, 37). In the eastern and northeastern part of the United States, *Ixodes scapularis* is the competent host of *B. burgdorferi*, and in the western part, it is *Ixodes pacificus*. In Europe, *Ixodes ricinus* is the predominant carrier of the spirochete (16). The life cycle of the tick plays an important role; without it, the bacteria could not be transmitted to its vertebrate hosts. The Additionally, this knowledge of this cycle is important for humans, as the tick is more likely to transmit *B. burgdorferi* at certain stages of its life cycle (38).

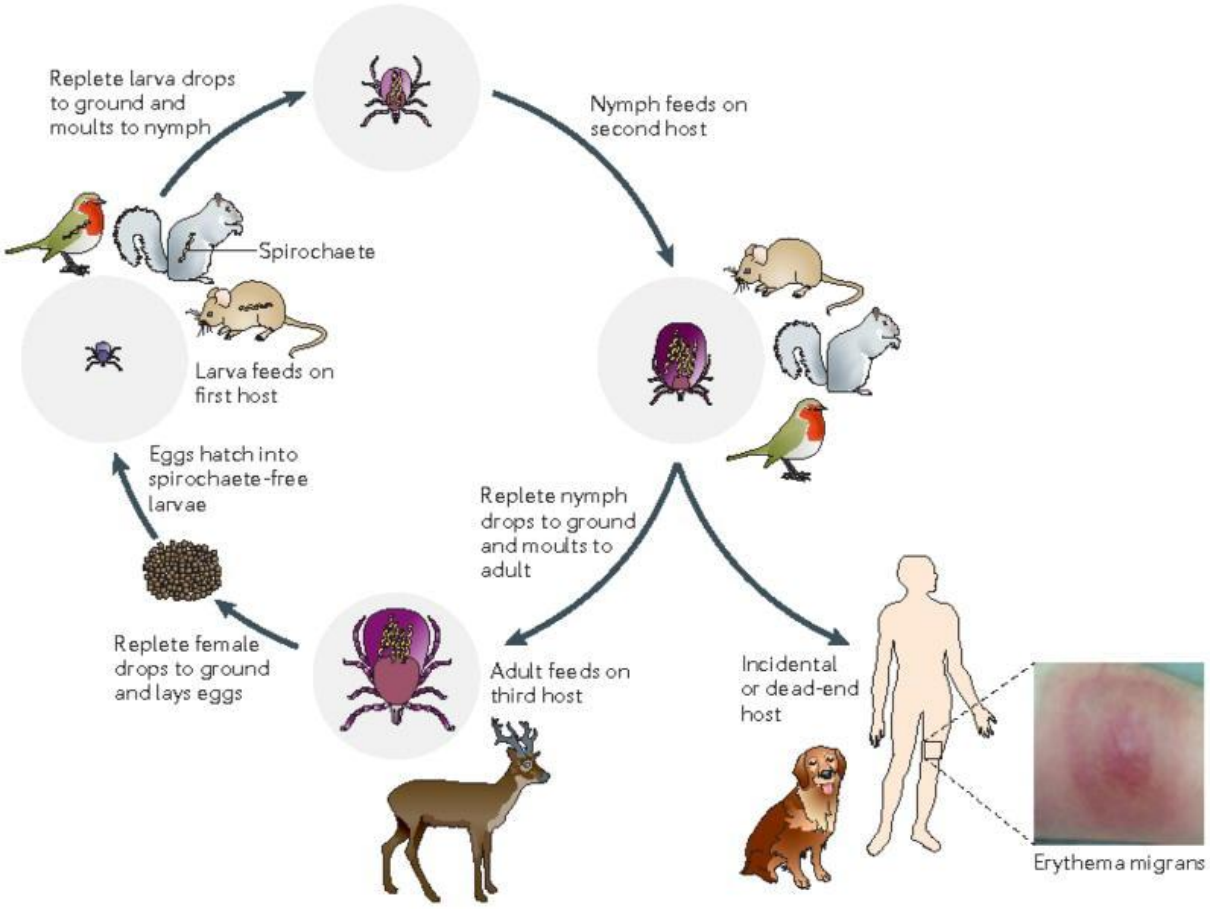

Figure 1: The life cycle of the *I. scapularis*. The diagram shows the cycle starting with the female ticks laying eggs. The newly hatched ticks will remain in the larval stage for a year. After taking a blood meal, it will molt into a nymph. The nymph aggressively looks for a blood meal, after which, it will molt into an adult. The adult will mate and lay eggs and the cycle starts over. Figure 1 is adapted from reference (16).

The *Ixodes* genus of ticks has a general life cycle to which they adhere (38, 39) (Figure 1). Ticks hatch from eggs as larvae. At this larval stage, the ticks are not infected with *B. burgdorferi* as transovarial transmission is absent in ticks (16, 40). In order to survive and acquire the spirochete, the larvae must take a blood meal in small vertebrates, such as mice and squirrels. If a tick's first host is infected with *B. burgdorferi*, then the ticks can also acquire the

infection from the host's blood that they ingest (40, 41). Once they acquire the infection, the spirochetes survive in the tick until it dies.

After their first blood meal, larvae molt into their next developmental stage, nymphs (16). The nymph will search for a second blood meal from an expanded list of hosts from that of the larvae, which includes slightly larger animals. It is at this stage that *Ixodes* ticks pose the greatest threat of transmitting *B. burgdorferi* to humans because of their possibility of being infected and their increased range of hosts (42). After feeding, the nymphs molt for a season, during which time they become adults (43). The adults prefer deer as their host, and it is on that host that they mate (41). After mating, the male dies and the adult female tick lays eggs. The cycle continues when the eggs hatch (39, 43).

1.3 Movement of *B. burgdorferi*

Motility is well characterized in *Escherichia coli*, thus it is a good model to which we can compare *B. burgdorferi*. *E. coli* is a motile organism with 5-7 peritrichous flagella per cell that extend out from the cell about 5 μm into the extracellular environment. Their flagella are helical and about 13.5 nm in diameter. Rotation of flagellar motors turns the flagella, enabling bacteria to propel themselves through liquid media (44). When *E. coli* cells sense a chemo attractant, they will turn their flagella in a counter-clockwise motion, causing them to run in a straight line. However, when they sense a repellant, or no longer sense an attractant, they will switch the direction that the motors spin. When the flagella spin clockwise, the cells tumble (45). Tumbling allows the cells to swim in a new direction. The flagella are more dynamic than originally thought; it seems that the flagella do not move in synchrony. In some cases, it can take as little as one flagella moving clockwise to throw the cell from its smooth run (46).

All members of the phylum spirochaete can be identified by a helical shaped cell. In contrast to *E. coli*, no flagella can be seen protruding from the cells into the extracellular space. This is due to the location of flagella in spirochetes; the flagella are in the periplasmic space (Figure 2A, B) (14). In *B. burgdorferi*, between 7 and 11 periplasmic flagella are anchored to each cellular pole forming a ribbon-like structure (47). The periplasmic flagella extend away from the poles of the cell, wrapping around the protoplasmic cell cylinder towards each other. The periplasmic flagella are crucial for *B. burgdorferi's* flat-wave morphology and motility (48). The *flaB* gene encodes the subunits that make up the major flagellar filaments (49). When *flaB* is inactivated, *B. burgdorferi* cells become rod-shaped and immobile, and are unable to establish infection in mice. This demonstrates the key role of the periplasmic flagella in the morphology, motility, and virulence of *B. burgdorferi.* Additionally, ticks artificially infected with the non-motile mutants failed to transmit the spirochetes into naïve mouse (19, 48).

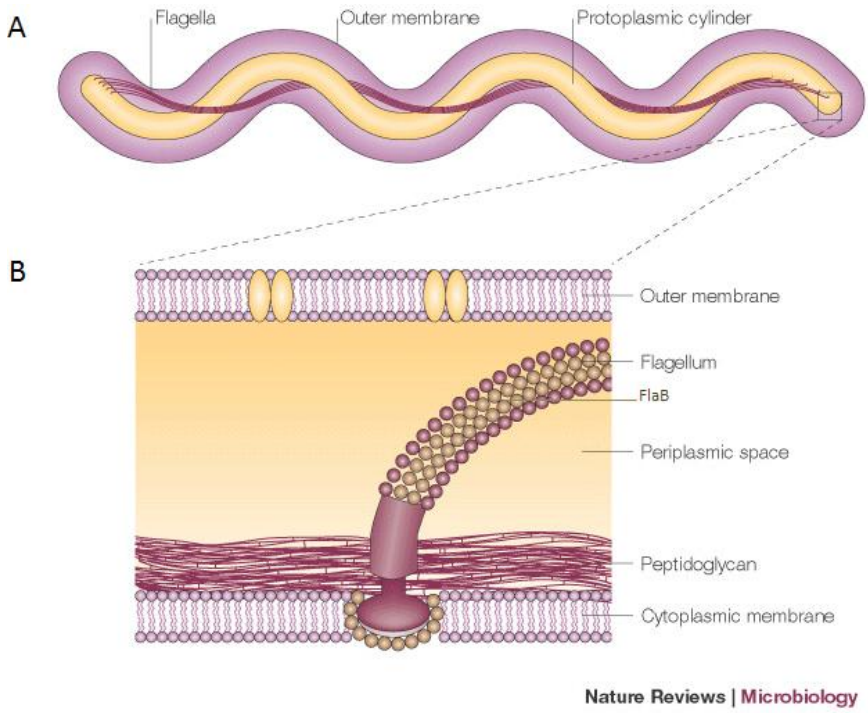

Figure 2. Schematic of periplasmic flagella. a) This graphic illustrates the location of the flagella in *Borrelia burgdorferi*. The flagella are internal to the outer membrane, but external to the protoplasmic cell cylinder. b) This cutaway graphic shows the periplasmic space in which the flagella filaments are located (92).

B. burgdorferi is an agile bacterium. While *E. coli* has only two swimming modes, *B. burgdorferi* has three swimming modes—it can swim forward, reverse, and flex (flexing is thought to be equivalent to tumbling). When the two ribbons of flagella, located one on each pole, spin with the same direction of rotation, the cell will flex. However, due to the left-handed helical shape of *B. burgdorferi*, when the periplasmic motors at the poles of the cell spin in opposite directions, the cell will swim in the direction of the pole that is spinning counter-clockwise (50). This asynchronous movement of the flagella seems to be a more complex chemotactic system than that of *E. coli*. *B. burgdorferi* does not favor swimming towards one pole over the other. It will reverse constantly and seemingly at random (51).

1.4 Chemotaxis Pathway of *Escherichia coli*

The chemotaxis pathway in *E. coli*, which allows it to sense a gradient in chemical attractants and repellents (52), is one of the most well studied in the bacterial domain. The signaling system has been studied since it was first elucidated in the 1970's (53). Because it is so well known, we will use its chemotaxis system as a model to understand *B. burgdorferi* chemotaxis.

E. coli's chemotaxis begins with the methyl-accepting chemotaxis proteins or MCPs (Figure 3) (53). MCPs are 40-65 kilodalton proteins that are embedded in the cytoplasmic membrane as dimers (54). *E. coli* has 5 MCP's, each for sensing different ligands in the environment (55). When the amino terminus of an MCP binds ligands in the periplasm, it undergoes a conformational change, sending a signal across the cytoplasmic membrane to the carboxyl terminus (55).

On the cytoplasmic side of the inner membrane, the MCP binds CheW and CheA. CheA, which is a dimer, functions as a histidine kinase (56). CheW functions as bridge between the MCP and CheA (Figure 3) (57). CheW transmits the signal with a conformation change from the MCP to CheA. A sensory subunit on CheA, which senses the signal from CheW, will then phosphorylate a neighboring subunit on CheA which is a histidine kinase (56). Mutants in either *cheW* or *cheA* will have flagella that only spin counter-clockwise, which will cause the bacteria to swim continually without tumbling (58).

After CheA auto-phosphorylates, CheA-P transmits its signal to a cognate response regulator CheY (59). In *E. coli*, CheY is a small, single domain protein. The phosphate is removed from CheA-P and placed preferentially on CheY's aspartate residue 57 (60). CheY,

upon phosphorylation, binds flagellar switch protein FliM, which is located at the base of the flagellar motor complex (Figure 3) (61). It is through FliM that the signal will be translated into physical action, ultimately causing the flagella to spin clockwise and the cell to tumble (61). To terminate the signal, CheY-P auto-dephosphorylates or a phosphatase, CheZ, binds to and dephosphorylates it with high affinity. This resets the signal back to default, and the flagella turn counter-clockwise (run) again. Both CheZ and FliM compete for the same position at the C-terminus of phosphorlyated CheY (62). Because CheY deficient mutants are unable to transduce the signal to tumble, the cell will continue on in the default swimming mode.

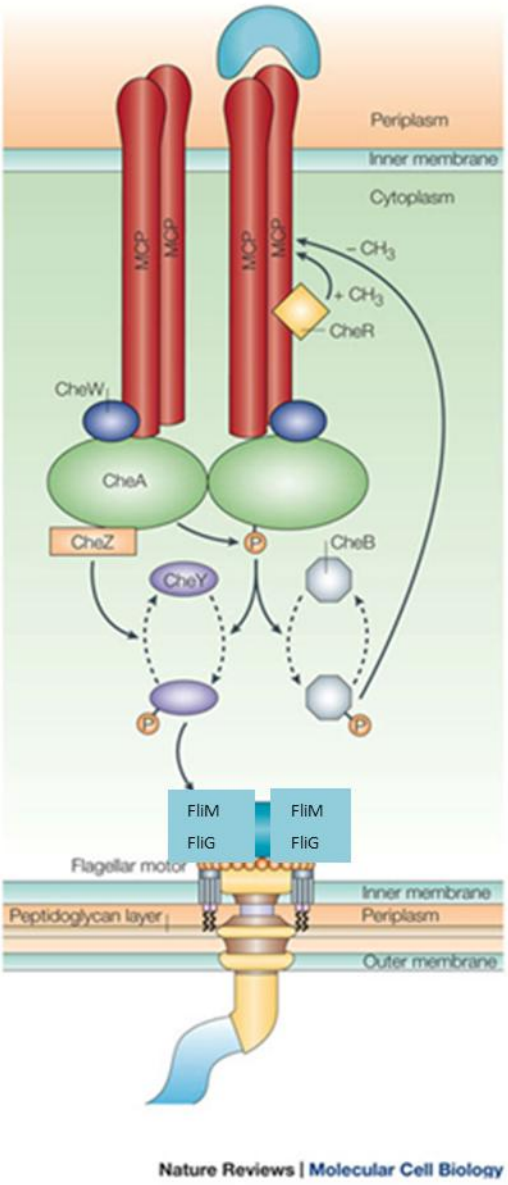

Figure 3: Graphical representation of the chemotaxis protein indicating their position and relative size in *Escherichia Coli.* The MCP sends a signal through CheW to CheA. CheA then phosphorylates CheY, which is the response regulator, moving the signal to the flagella at FliM. In this case, the ligand has just been released, so the phosphorylation of CheA and CheY occurs (98).

CheB is a methylesterase that catalyzes the hydrolysis of γ-glutamyl methyl ester residues on the MCPs, resulting in the release of methyl groups in the form of methanol. CheB

is phosphorylated by CheA-P, which activates it. CheR is the antipode to CheB. CheR is a methyltransferase that only methylates membrane bound MCPs (63). This is part of the environmental sensory adaption system, as the methyl-groups decrease the efficiency of ligand binding by the MCP (64). While CheB is removing methyl groups from an MCP, CheR is replacing them back on the MCP (Figure 4). Deletion mutations in *cheR* cause counter-clockwise flagella rotations so that the cell will swim continuously, without tumbling (58). A mutant that is unable to produce functional CheB will constantly tumble, indicating that the removal of the methyl groups activates the MCP and starts signal transduction (58). Different MCPs can carry different amounts of methyl groups. For example, MCPI can carry six, but MCPIV carries up to four (64).

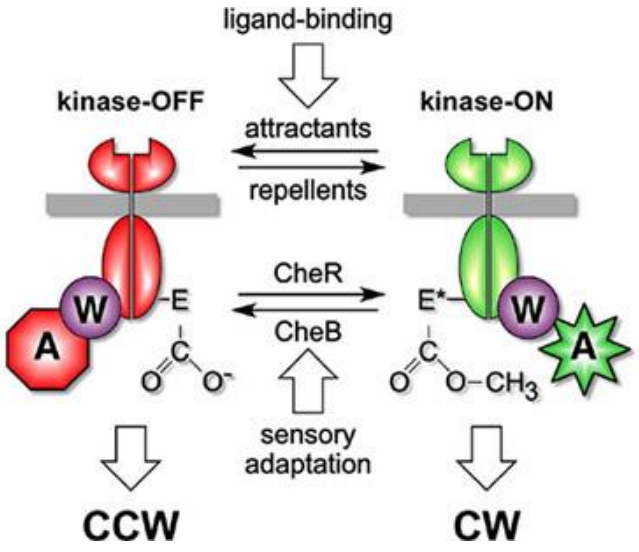

Figure 4: Graphical representation of the relationship between the MCP/CheW/CheA structure and the methyl group manipulation of CheR and CheB. When an attractant is bound and the MCP is methylated, CheA will not be active and the flagella will turn counter-clockwise and the cells run (97).

1.5 Chemotaxis pathway of *B. burgdorferi*

Chemotaxis is hypothesized to be a virulence-associated factor of *B. burgdorferi*. More than one report indicates that chemotaxis is important for this spirochete's pathogenesis (14, 17). As mentioned earlier, *B. burgdorferi* deviates from *E. coli* in several important ways in its swimming modes and cellular structure. There are also some differences in their chemotactic pathways. A more complex chemotactic system would be expected from *B. burgdorferi*. This expectation is realized with genomic analysis revealing that *B. burgdorferi* has more than one copy of several chemotactic genes: two *cheA*, three *cheW*, three *cheY*, two *cheB*, and two *cheR*. Some of these homologues still have unknown functions (65). *B. burgdorferi* does not encode a homologue for phosphatase CheZ but instead possess a CheX (66).

B. burgdorferi has five putative methyl-accepting proteins, named MCP1-5, located on the genome at*: bb0578, bb0596, bb0597, bb0680,* and *bb0681*, respectively (15). MCP3 and MCP5 share homology with the most abundant *E. coli* MCPs (*tar* and *tsp*) (67). By tagging these proteins with green fluorescent proteins and immunofluorescence assays, it has been shown that *B. burgdorferi* MCPs cluster near the periplasmic flagellar motors at the poles of the cells. This localization may help in the speed of signal transduction from the MCPs to the flagella motors (68).

Genes which encode proteins that work in collaboration are often clumped together in the same operon. One such operon in *B. burgdorferi* pertaining to chemotaxis consists of the following genes: *flaA (bb0668*), *cheA2 (bb0669*), *cheW3 (bb0670*), *cheX (bb0671*), *cheY3 (bb0672*). All of the genes in this operon have chemotaxis related functions, except *flaA*, which encodes a subunit that makes up the outer layer of the periplasmic flagella filament (69) . When

a loss-of-function mutation occurs in *cheA2*, *cheX*, *cheY3*, or *cheW3*, the result is non-chemotactic bacteria (60, 66, 70, 71).

CheA2 of *B. burgdorferi* functions similar to that of *E. coli* in that it is a histidine kinase that binds nucleotides. A loss-of-function mutation in this *cheA2* results in a phenotype that constantly runs, whereas a loss-of-function of *cheA1* has no discernible phenotype (60). CheA2 is an 864-amino-acid protein that shares 35.5 percent similarity with the *E. coli* CheA (15). Using immuno-precipitation assays, CheA2 has been shown to associate with both CheW1 and CheW3 and CheA1 has been shown to associate with CheW2 (70). Another difference between *B. burgdorferi* and *E. coli* is that CheW3 is almost three times bigger than *E. coli's* 18 kD CheW (72), (73). Based on the results, it appears that when the MCP undergoes a conformational change, CheW3 transduces the signal to CheA2, which auto-phosphorylates and then phosphorylates CheY3 (66). CheX then dephosphorylates CheY3-P (66, 71).

B. burgdorferi has three *cheY* genes with homology to *E. coli's cheY: cheY1, cheY2, and cheY3.* The *B. burgdorferi cheY* genes are numbered in order of their locus number; *cheY1* is locus *bb0551*, *cheY2* is *bb0570,* and *cheY3 is bb0672* (74). The functional residues of the CheY molecule of *E. coli* are conserved within the three *B. burgdorferi* CheY molecules (Figure 5). In a non-virulent strain of *B. burgdorferi* (B31A), *cheY1* and *cheY2* mutants showed normal swimming motility and chemotactic response using capillary tube and swarm plate chemotaxis assays (74). *cheY3* mutants, on the other hand, exhibited a significantly reduced chemotactic response (74). While it was reported that all three CheYs were able to be phosphorylated by CheA1-P or CheA2-P, only CheY3-deficient *B. burgdorferi* exhibited a phenotype that differed from wild type *in vitro* (74). Taken together, this evidence indicates that CheY3 is the main chemotactic response regulator under the conditions tested.

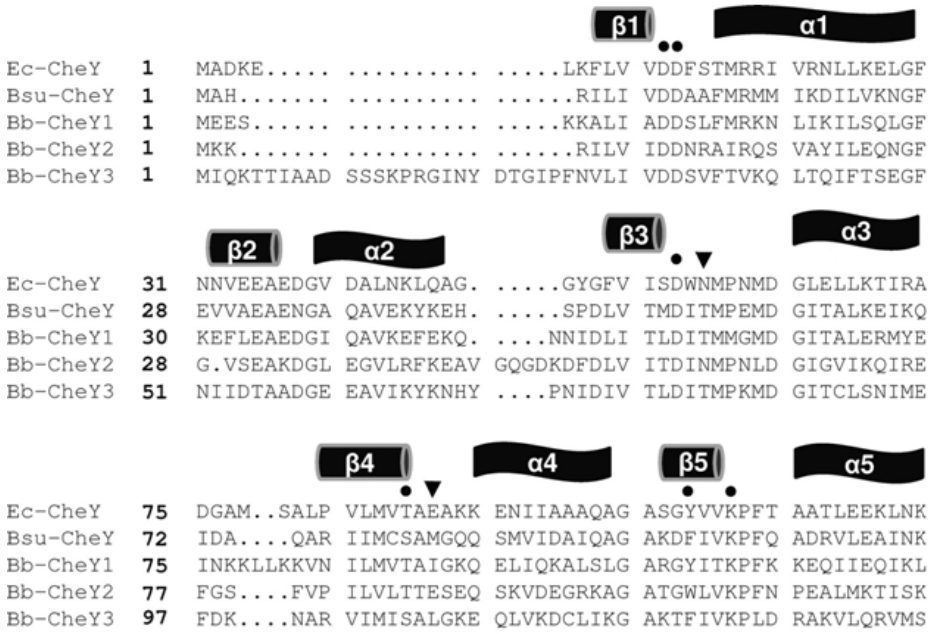

Figure 5. T-Coffee amino acid sequence alignments of CheY molecules from *B. burgdorferi*, *E. coli*, and *Bacillus subtilis*. Circles indicate conserved residues that are essential for function in *E. coli*. The triangles indicate active-site residues of *E. coli* CheY, N59 and E89, which are conserved in *B. burgdorferi* CheY2, but not in CheY1 or CheY3. Secondary structures for *E. coli* CheY, which are expected for *B. burgdorferi* CheY proteins, are above the sequence alignment. The *E. coli* and *B. subtilis* CheY proteins are denoted as Ec-CheY and Bsu-CheY, respectively. Indicated on the left are amino acid residue numbers (74).

While there is currently a strong effort to study genetics of spirochete chemotaxis, still no model exists for the actual mechanics related to the independent movement of the periplasmic flagella at each poles.

Δ*cheY3* mutants are non-chemotactic *in vitro*. Their phenotype is that of constantly running cells (71). While we hypothesize that these cells would be non-virulent, there is no data to conclusively demonstrate this. When the other two *cheY* genes are inactivated, the cells display a wild type level of motility and chemotaxis *in vitro*. However, *cheY1 and cheY2* express in growing *B. burgdorferi* and as indicated above, they are also phosphorylated by the histidine kinases, thus we predict that cheY1 and cheY2 could function *in vivo*. In a pilot transposon

mutagenesis study, a *cheY2* mutant was shown to be necessary for viability within a mouse (75). It is not known whether *ΔcheY2* mutants can survive in the ticks or if they are important for transmission from the tick to the mouse. As we believe that *cheY1* and *cheY2* have a function *in vivo*, we want to use mutants of these genes in a tick-mouse cycle experiment to determine, if they have function at a particular point in the cycle.

1.6 Flagellar Structures

The chemotaxis signal is transferred into physical motion at the stator in the flagella apparatus. The stator in *Borrelia burgdorferi* is made up of MotA and MotB. These proteins are predicted to contain transmembrane domains (76). Cryo-electron tomography (cryo-ET) confirms that the stator forms a ring around the rotor at the cytoplasmic membrane and is directly external to the C-ring. The stator is the motor that turns the rotor (77) (Figure 6).

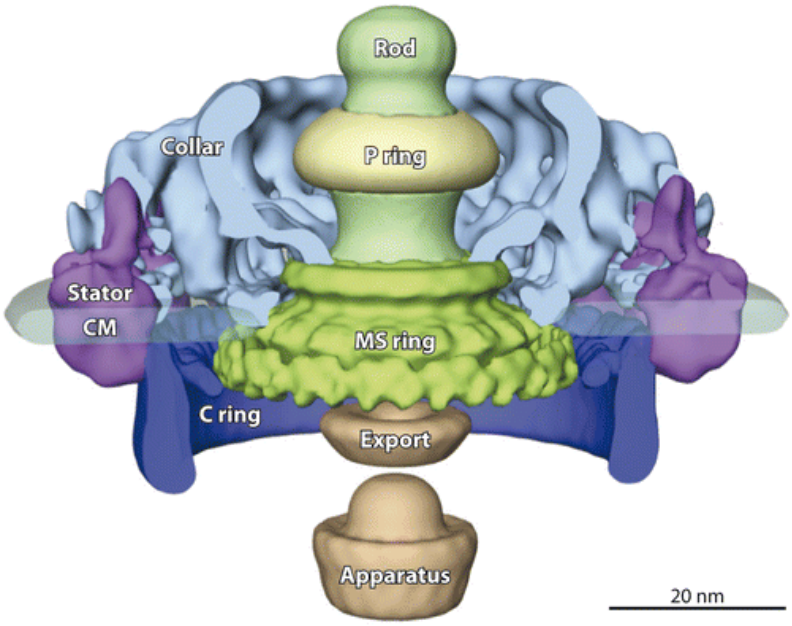

Charon NW, et al. 2012.
Annu. Rev. Microbiol. 66:349–70

Figure 6. 3-D model of the basal body of a *B. burgdorferi* flagella motor based on Cryo-ET images. This model shows the export apparatus at the base of the basal body, on which sits the MS ring. These are surrounded by the C-ring and the stator. On top of the MS ring are the rod and the P-ring, which are surrounded by the collar (80).

In between the rotor and the stator is a protein, FliL, which may be involved in flagellar orientation (74). The rotor is made up of the C-ring (FliG, FliM, FliN). At the distal end of the rod is the hook protein (FlgE), from which the flagellum extends, wrapping around the body of the cell (78). When the stator rotates the rotor, the hook turns with it, thereby spinning the periplasmic flagella (FlaA and FlaB).

1.7 The Collar Structure

Sitting on top of the stator and extending through the peptidoglycan layer is a predominant structure known as the collar (Figure 7). This collar wraps around the p-ring, which is thought to act as a bushing for the rod as well as help maintains the periplasmic flagellar normal orientation toward the cell body (77). The collar structure, though appearing circular, actually creates more of an ellipsis shaped ring around the p-ring (figure 21B) (79). The narrowest diameter is 35 nm and the longest diameter of the elliptical ring created by the collar is 38 nm (79). The elliptical shape is most likely due to curvature of the membrane in which the flagella motor is embedded (79). The collar appears to be connected to the MS ring and the stator. This structure is unique to spirochetes and its exact function is unknown (80). The gene or genes coding the collar structure have not been identified yet. We plan to find these genes through Bioinformatics techniques. By comparing the *B. burgdorferi* genome to suspected genes known from the literature, we plan to discover the genes encoding the collar structure and confirm this through gene inactivation and cryo-ET.

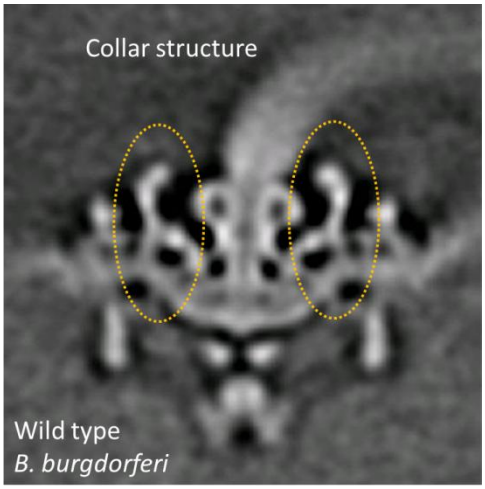

Figure 7. Cryo-ET image of the cross-section of the basal body of *B. burgdorferi*. The collar structure is indicated by the orange ellipsis. Image created by Jun Liu and Xiaowei Zhao from the University of Texas at Houston.

1.8 Flagellar Assembly

Most of the flagellar genes are located in a large 27 gene *flgB* operon (81). The majority of these genes have been or are being characterized in our laboratory, however *fliZ* has yet been characterized. These genes encode the export apparatus (*fliP, fliQ, fliR, flhA,* and *flhB*), the C-ring (*fliG, fliM,* and *fliN*), and the stator (*motA*, and *motB*). *fliZ* is located in the middle of this *flgB* operon. In *Salmonella*, the homolog for the *B. burgdorferi fliZ* is called *fliO* (82). While FliZ shares only 28% amino acid sequence identity with FliO in *Salmonella enterica* serovar Typhimurium str. D23580's, the functional domains of FliO are conserved in FliZ (67). In *S. enterica*, a deletion of *fliO* creates a severely slow mutant. When *fliO* is inactivated, the motile phenotype can be saved by constitutive expression of *fliP*. This indicates that *fliO* is a regulator of *fliP* (83). It is our hypothesis that we would see a similar slow mutant in *B. burgdorferi*.

CHAPTER 2: MATERIALS AND METHODS

2.1 Bacterial strains and growth conditions

Two strains of *Borrelia burgdorferi* were used in this study: high-passage avirulent *B. burgdorferi* strain B31A and low-passage, virulent *B. burgdorferi* strain B31A3. The main difference between these is that the virulent B31A3 strain contain all 21 plasmids except a 9 kb circular plasmid (cp9), whereas the B31A strain has lost 11 plasmids. Both strains have the 910 kb chromosome (12). Two strains are used rather than just one, because the avirulent strain is genetically more malleable and durable for *in vitro* experimentation than the virulent strain. *B. burgdorferi* was grown in BSK-II medium at 35^{o}C in an incubator with 2.5% CO_2. Plating BSKII (P-BSKII) medium was prepared with 0.6% agarose (84).

2.2 *cheY2* inactivation

To inactivate *cheY2*, we PCR amplified a 1494 bp section of genomic DNA using Dream Taq po Lymerase (Fermentas Inc.) using primers, TCTGCTAGGTTTCAAAATAT (Y2-KO-F-2) and TGGACTTACCCT TTACATAG (Y2-KO-R-2). This fragment encompassed a 658 bp section upstream of *cheY2*, a 493 bp section downstream of *cheY2,* as well as the 375 bp *cheY2* gene. The 1494 bp fragment was inserted into pGEM®-T Easy vector system using TA cloning, and then restriction digested with HindIII in order to ligate a kanamycin antibiotic resistance cassette. An *aph1* (encodes kanamycin resistance) gene was fused to the *B. burgdorferi flgB* promoter (P_{flgB}-*aph1*) in order to express the resistance gene in *B. burgdorferi* which was then inserted into HindIII site of the target gene. The orientation P_{flgB}-*aph1* is in the same direction as the transcription of the target gene (Figure 8).

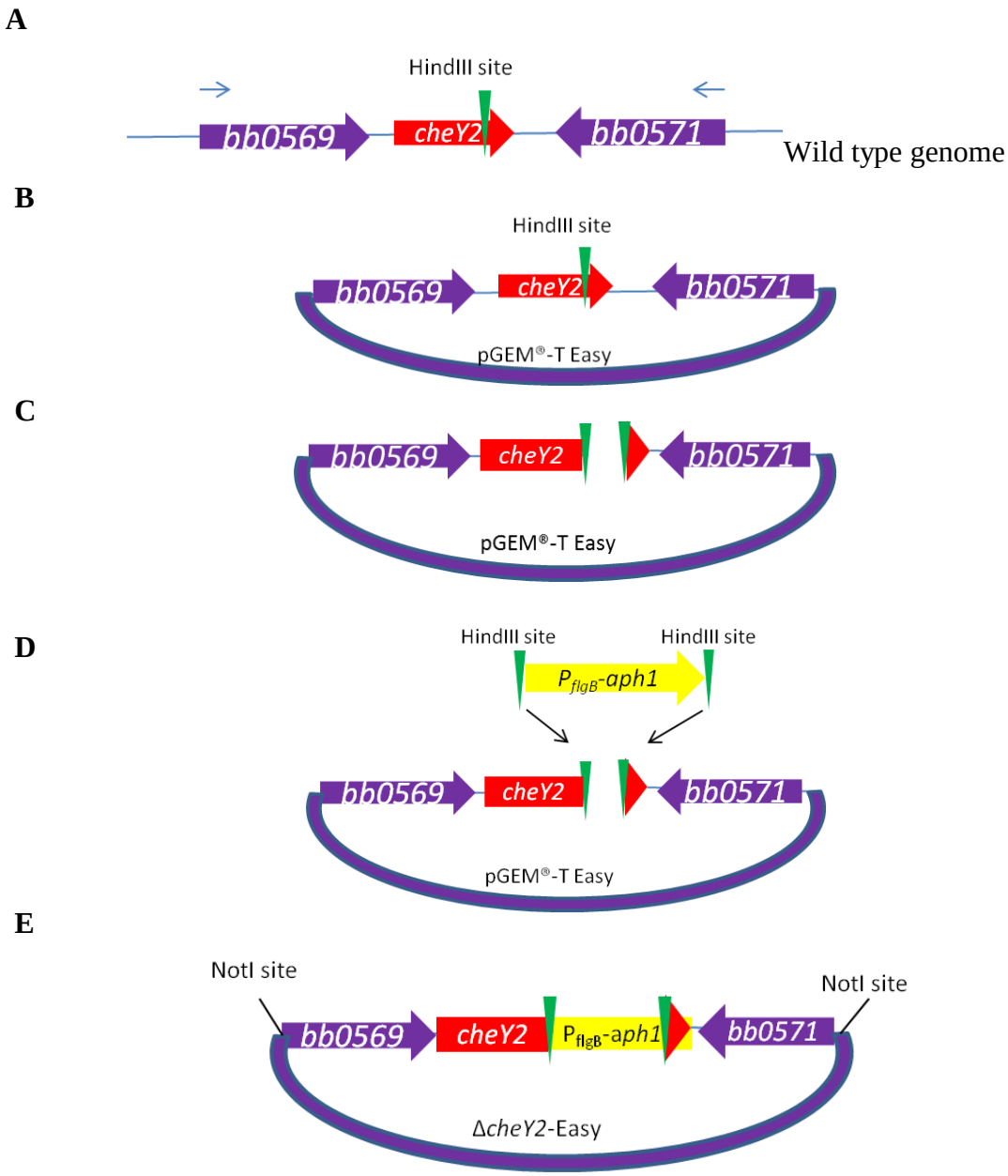

Figure 8. Schematic representation of the construction of *ΔcheY2*-Easy plasmid. A) Step 1: Amplify fragment of genomic DNA encompassing *cheY2* (the blue arrows represent location of primers used for this step). B) Step 2: Insert fragment into pGEM-T Easy vector. C) Step 3: Restriction digest at the HindIII site. D) Ligate P_{flgB}-*aph1* to the HindIII. E) Completed plasmid. Step 5: Digest the plasmid with NotI and use the linearized cheY2-P_{flgB}-*aph1* DNA to electroporate in competent *B. burgdorferi*.

The plasmid, Δ*cheY2*-Easy, was transformed into *E. coli* strain JM109 and then isolated from single colonies using Wizard® Plus Midipreps DNA purification system (Promega Inc.). 80 µg of the purified plasmids were digested with NotI, ethanol precipitated, and rehydrated in 15 µL of nuclease-free dH_2O. The resulting linear DNA was used for electroporation into competent *B. burgdorferi* B31A3 cells and allowed to recover overnight. The electroporated cells were diluted in 100 milliliters of BSK-II with 200 µg/ml of kanamycin and plated in 96-well plates with 200 µl of media per well. Plates were incubated for 2-4 weeks in an incubator. A color change in the wells indicated kanamycin resistant bacterial growth. Some of the randomly picked clones were grown in 3 ml BSKII, and 1.5 milliliters of the culture was mixed with 0.5 milliliters of glycerol and frozen at -80^{o}C for stock. The remaining 1.5 milliliters was used for extraction of genomic DNA using Promega's PureYield™ Plasmid Miniprep System. This DNA was used for genotyping as well as checking retention of endogenous plasmids by PCR. Genotyping was conducted with the primers used in the creation of the plasmid, (Y2-KO-F-2) and (Y2-KO-R-2). This genotype was also confirmed with a primer that binds to the *aph1* cassette, TGTTTCTGAAACATGGCAAAGGTAG (BKAN-1), and a primer that binds to a small portion of *cheY2* that was not deleted, GATGACAATAGGGCA ATAAG (Scr-CheY2-F). Once a clone is confirmed as mutant, endogenous plasmids were detected using previously described primers (9). Retention of those plasmids is important for infection and persistence in the host (12). Additionally, western blotting using specific antisera was also used to confirm the inhibition of CheY2 protein in the mutant cells (see below).

2.3 *cheY1* inactivation

To inactivate *cheY1* (381 bp gene), a 2292 bp section of *B. burgdorferi* genomic DNA was PCR-amplified using Taq DNA Po Lymerase and primers, GCAGTTGTTTTATGACATTGTC (Y1-KO-F-Big) and ATCTTGTCGGAAAACCCTTC (Y1-KO-F-Big). This DNA fragment encompassed *cheY1* as well as a 1569 bp upstream and a 342 bp downstream of *cheY1*. The PCR amplified DNA was inserted into pGEM®-T Easy Vector. A 273 base pair section was deleted from *cheY1* using two HindIII sites within the *cheY1* gene. A P_{flgB}-*aph1* cassette was then inserted between the HindIII sites within the *cheY1* gene oriented in the same direction as the target gene creating the pGEMT-Δ*cheY1* plasmid (Figure 9).

A

B

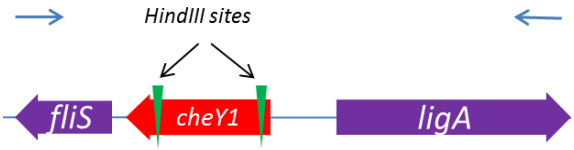

C

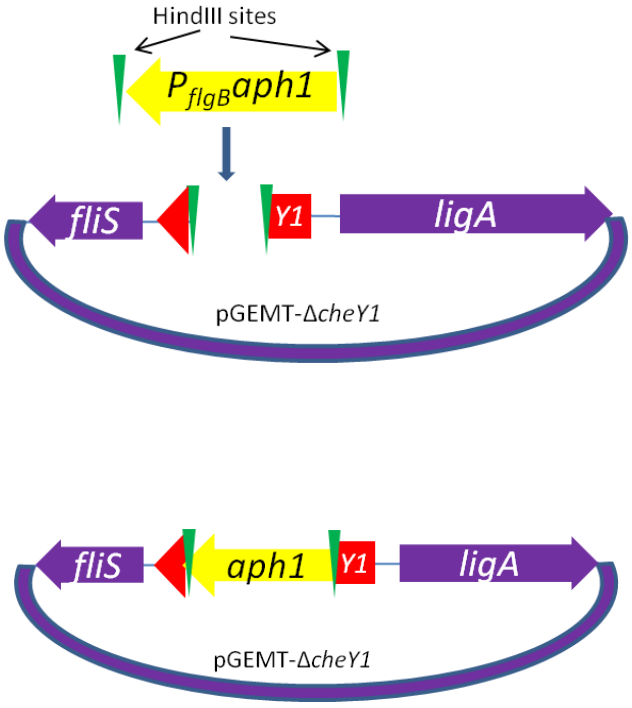

Figure 9. Schematic representation of the construction of *ΔcheY1* plasmid. A) Step 1: Amplify fragment of genomic DNA encompassing *cheY1* (the arrows represent location of primers used for this step). B) Step 2: Insert fragment into pGEM-T Easy vector. C) Step 3: Digest at the HindIII sites and ligate P_{flgB}-*aphI* to the same sites. C) Completed plasmid, pGEMT-Δ*cheY1*.

We electroporated the pGEMT-Δ*cheY1* plasmid into competent, virulent *B. burgdorferi* stain: B31A3 cells. Transformants were genotyped using the primers used in creation of the plasmid as described before. Retention of endogenous plasmids was checked by PCR to ensure that these cells were virulent.

2.4 *bb0526* inactivation

In order to make the *bb0526* mutant, a 4251 base pair section of wild type genomic DNA, centered on *bb0526* (1824 bp), was amplified using Dream*Taq* po Lymerase and the following primers ACTAGGCTTGCATTAAGTGG (bb0526-KO-F) and GGCCTTATACTTTGAAAACC (bb0526-KO-R). This genomic DNA included a section 1568 base pairs upstream and 1510 base pairs downstream. This section was inserted into pGEM®-T Easy Vector. Within the *bb0526* gene, there are two HindIII sites, which were used to restriction digest a 1161 base pair section out of the gene. In place of this section we inserted promoterless *aph1* (also confers kanamycin resistance) (Figure 10) (85).

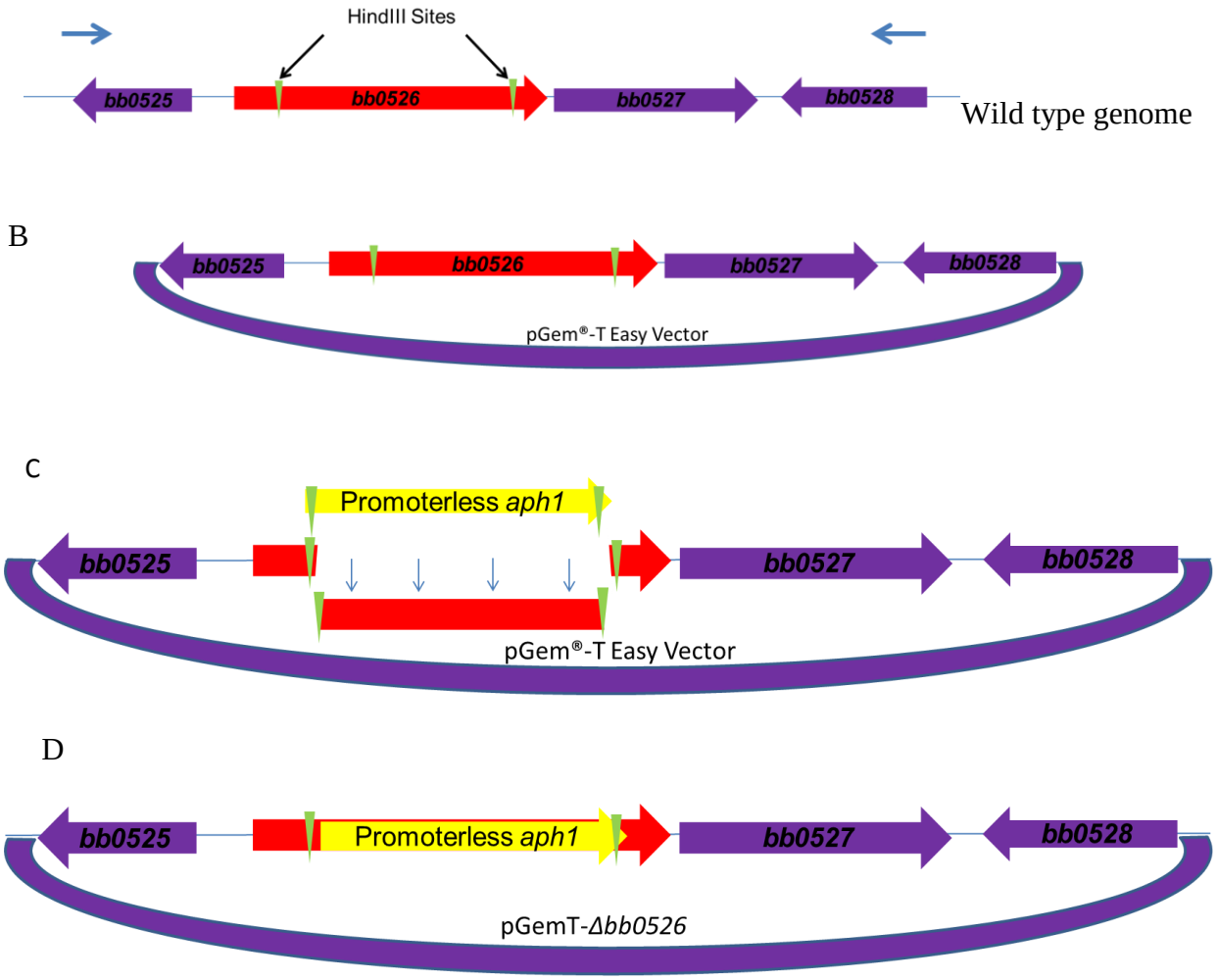

Figure 10. Schematic representation of the construction of *Δbb0526* vehicle. A) Step 1: Amplify fragment of genomic DNA encompassing *bb0526* (the arrows represent location of primers used for this step). B) Step 2: Insert fragment into Promega's pGEM®-T Easy vector. C) Step 3: Restriction digest the HindIII sites and ligate P_{flgB}-*aph1* to the plasmid at the HindIII sites. C) Completed plasmid, pGemT-Δ*bb0526*.

Mutants were made in both strains, B31A and B31A3. For genotyping, the entire construct was amplified by PCR with bb0526-KO-F and bb0526-KO-R. Plasmid retention was checked for the mutants in B31A3 strain.

2.5 Complementation of *bb0526 in cis*

Complementation of the *bb0526* mutant was done by genomic reconstitution. The complementation vehicle was created by joining three fragments: parts 1, 2, and 3 (Figure 11). Using primers GGCCTACTTTTCTTTTGTAGG (bb0526Comp P1F) and ACCGGTACAAATATTTCAATTAACAAAC (bb0526Comp P1R), part 1 was amplified as a section of *B. burgdorferi* genomic DNA which included *bb0525, bb0526* and *bb0527*, (Figure 11A) using Expand Long Template PCR System (Roche Inc.). The second primer engineered an AgeI site at the end *of bb0527*. Part 1 was inserted into *TOPO® XL* PCR Cloning Kit (Figure 11B). Using primers ACCGGTCTTCAAGGAAGATTTCCTAT (bb0526Comp P2F) and AACTTTAAAAGACGTCATTATTTGCCGAC (bb0526Comp P2R), part 2 was amplified from an *aadA* (spectinomycin and streptomycin resistance) cassette (Figure 11C). The primers of part 2 engineered an AgeI site upstream and an overlapping region with fragment 3 downstream (Figure 11D). Part 3 was amplified from *B. burgdorferi* genomic DNA downstream of the *bb0526* using these primers: CTTTTAAAGTTTTAAATTTTTTTGTTAAATAAAT (bb0526Comp P3F) and CTGCAGGTGAATAATCTTAAAGACAAG (b0526Comp P3R). These primers engineered overlap with part 2 on one side and a PstI site on the other (downstream) end (Figure 11D). Part 2 and part 3 were connected using overlapping PCR and this overlap product was inserted into pGEM®-T Easy Vector (Figure 11E). The AgeI and PstI sites were used to digest the overlap fragment (part 2 and part 3) product from the vector (Figure 11G). Part 1 was then restriction digested with AgeI and PstI (Figure 11F) and into these sites we inserted the overlap fragment.

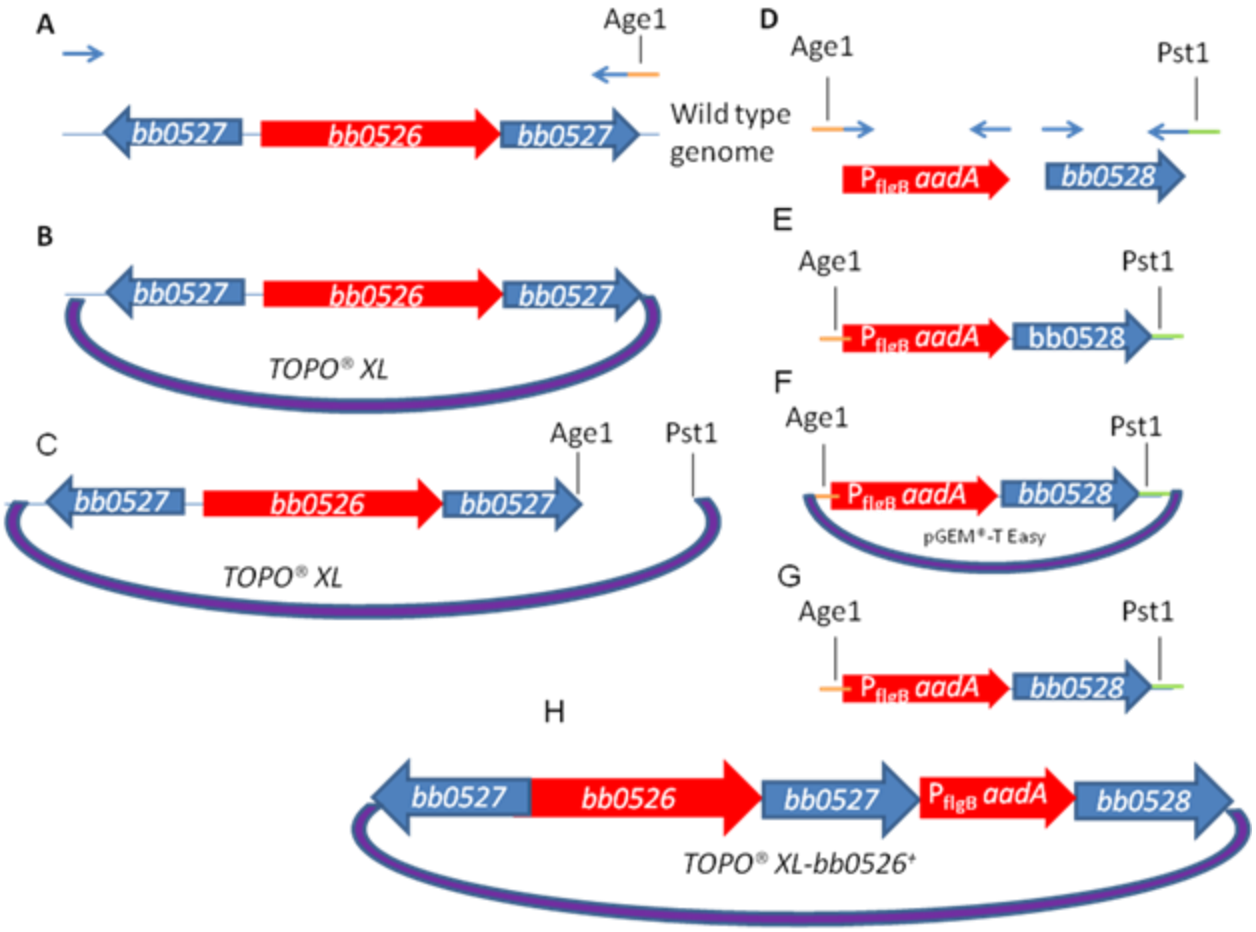

Figure 11. Schematic representation of the construction of Δ*bb0526* complementation vehicle. A) Step 1: Amplify part 1 fragment from genomic DNA encompassing *bb0526* and *bb0527* (the blue arrows represent location of primers used for this step). The reverse primer has an AgeI engineered into the tail. B) Step 2: Insert fragment from the previous step into *TOPO® XL*. C) Step 3: Amplify fragment of genomic DNA encompassing *bb0528* (part 3) and P_{flgB}-*aadA* (part 2) (the blue arrows represent location of primers used for this step). The primers used in this step were engineered to add an AgeI site upstream of P_{flgB}-*aadA* and a PstI site downstream of *bb0528*. D) Using overlapping PCR, join the P_{flgB} *aadA* fragment and the *bb0528*. E) Insert the fused fragment into pGEM®-T Easy Vector. F) Cutting at the engineered sites, remove the fused fragment from pGEM®-T Easy Vector and cut the previous plasmid with the same enzymes. G) Ligate the fused fragment into the *TOPO® XL* fragment for a finished product, *TopoXL-bb0525*$^{+}$.

B31A3 and selected for with streptomycin. Resistant colonies were isolated for genotyping.

Primers AACTTAAATATATTTTTTTTAAAAGAT (Rbb0526 F) and

TTATTCATAAATATTTATTTTTTTTGC (Rbb0526 R) were used to differentiate between wild type/complement and mutant *bb0526.* Primers b0526Comp P2F and b0526Comp P3R were used to determine the presence of the *aadA.* In the B31A3 strain, endogenous plasmids were confirmed as previously described.

2.6 Inactivation of *fliZ*

The *fliZ* mutant was made by replacing *fliZ* (*bb0276;* 676 bp) with a promoterless *aph1* cassette using overlapping PCR from three PCR products (Figure 12). Part one amplified from upstream of *fliZ* using CATTTCTGTAGGGGGAACTATTTGAGC (fliZ-P1F) and ATTAAAACTAAAAATGAATAATAATAGTTA (fliZ-P1R). Part two was amplified from promoterless *aph1* cassette and was engineered with overlapping regions on each parts one and three using primers ATCTATCTTTTAGAAAAACTCATCGAGCATC (fliZ-KOF) and TGAATAATAATAGTTAAAAGCAATTTTAAATG (fliZ-KOR). Part three was amplified from genomic DNA downstream of *fliZ* using primers TTTTCTAAAAGATAGATTAAAAAAATTTTAG (fliZ-P2F) and GGCAAAGATATCATCACAGGGGGCAAC (fliZ-P2R) (Fig. 12A). Using overlapping PCR and primers fliZ-P1F and fliZ-KOR, the first part was joined to the second (Fig. 12B). The joined segments were then connected to the third part using primers fliZ-P1F and fliZ-P2R. The final 2423 bp product was then inserted into pGEM®-T Easy Vector (Fig. 12C and 12D).

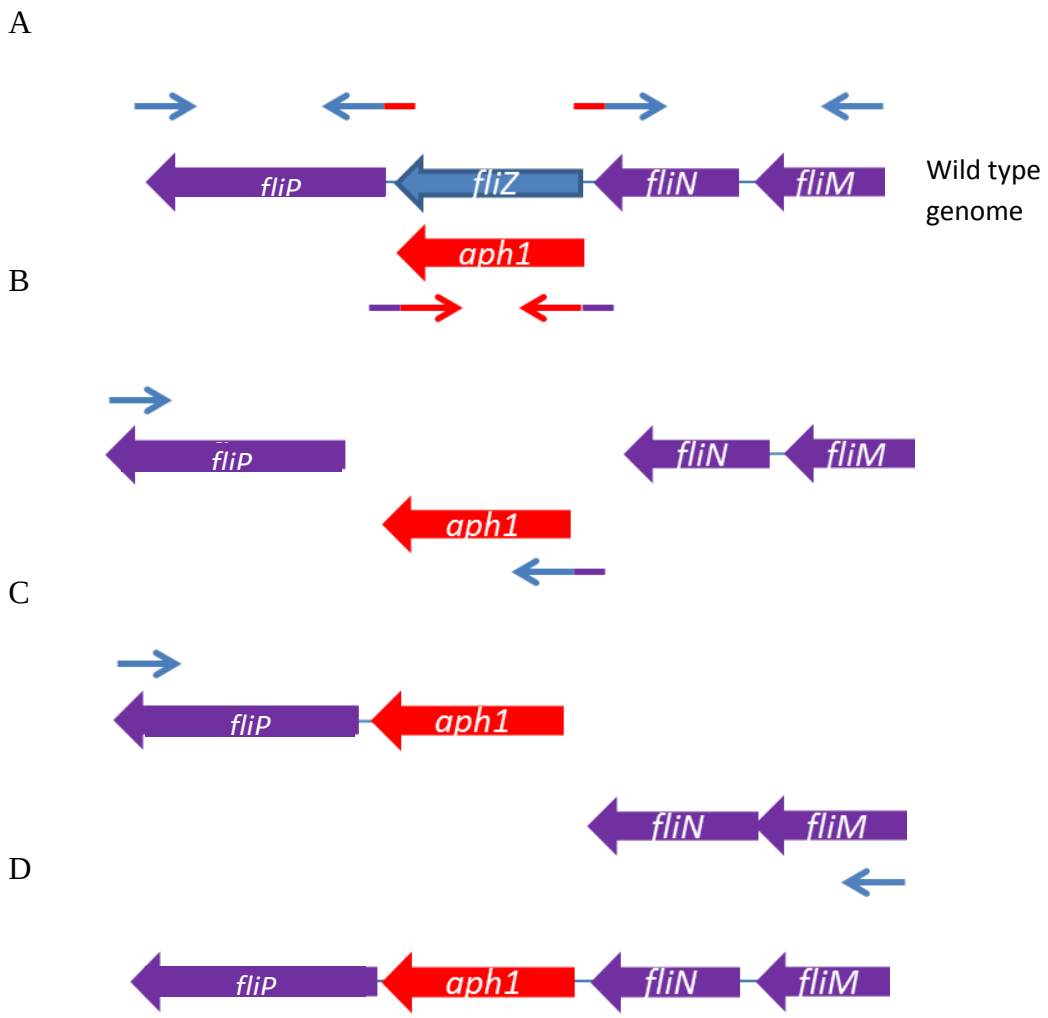

Figure 12. Schematic representation of the construction of Δ*fliZ* vehicle. A) Step 1: Amplify DNA fragments with paired primers. B) Join the first two fragments using overlapping PCR. C) Connect the third fragment to the first two using overlapping PCR for the completed product (D).

Electroporation was done as previously described into *B. burgdorferi* B31A. Genotyping of the *fliZ* mutants was done with fliZ-P1F and fliZ-KOR.

2.7 Complementation of *fliZ in trans*

In order to complement the *fliZ* mutant *in trans*, the target gene was fused to its native *flgB* promoter (P_{flgB}) using overlapping PCR (Figure 13). P_{flgB} was amplified from genomic DNA with primers GTCGACCCCGAGCTTCAAGGAAG (PflgB-F) and

TATTCATGAAACCTCCCTCATTTAAAATTGC (PflgB-R). Primers GAGGTTTCATGAATAATAAATTTTTATTTTTAGTTT (fliZ-F) and GGATCCCTAAAATTTTTTTAATCTATCTTG (fliZ-R) were used to amplify *fliZ* from genomic DNA. These two DNA fragments was amplified by overlapping PCR which creates a SalI site at the 5'- and a BamHI site immediately downstream of *fliZ*. The construct was then inserted into pGEM®-T Easy Vector. The resulting plasmid was then restriction digested with BamHI and SalI, as was the pBSV2G shuttle vector. Ligation of the two restriction digested fragments resulted in pBSV2G-*fliZ*$^{+}$.

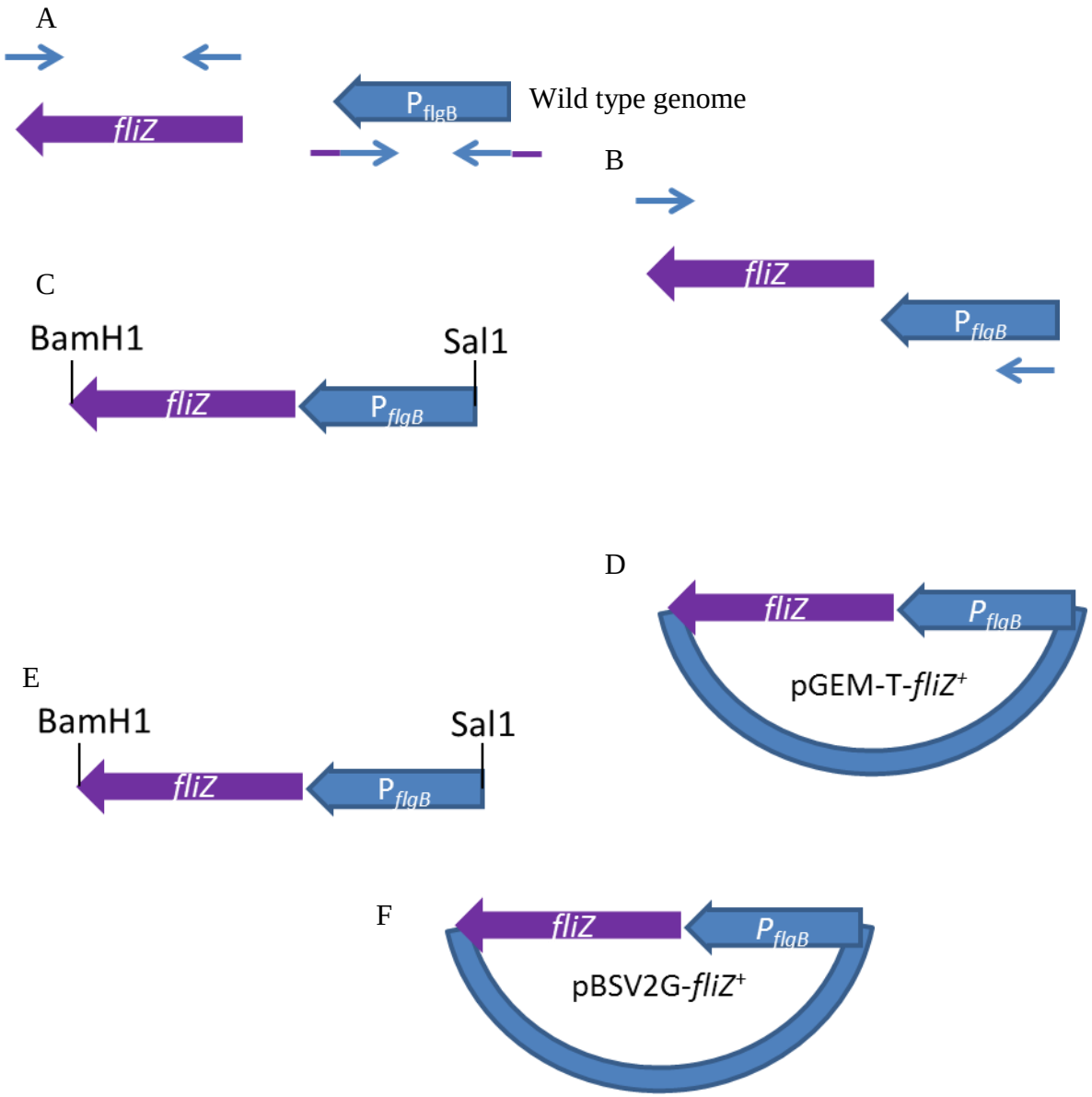

Figure 13. Schematic representation of the construction of Δ*fliZ* complementation vehicle. A) Step 1: Amplify DNA fragments with paired primers. B) Step 2: Join the first two fragments using overlapping PCR to get (C). D) Step 3: Ligate overlapping product into pGEM®-T Easy Vector. E) Digest the PCR product out with *BamH1* and *Sal1*. F) Ligate into pBSV2G for finished product.

The pBSV2G-*fliZ*$^{+}$ plasmid was electroporated in the *B. burgdorferi* B31A Δ*fliZ* strain and plated in to 96-well-plates with gentamicin and kanamycin. Resistant clones were genotyped using PfligB-F and fliZ-R.

2.8 Plasmid rescue assay for *fliZ* complement

In addition to genotyping, the presence of pBSV2G-fliZ$^+$ plasmid in the complemented *fliZ* (*fliZ*$^+$) cells were confirmed by plasmid rescue as follows. *fliZ*$^+$ complement cells were grown in BSK-II media supplemented with 40 µg/ml gentamicin plus 200 µg/ml kanamycin. As the cells reached mid-log phase, two ml of the cells were aliquoted into an Eppendorf tube, and the cells were spun down and washed with phosphate buffer saline (PBS) thrice. DNA was then isolated and purified from the *B. burgdorferi* cells using the plasmid Miniprep kit as above. 10 µL of this DNA was then transformed into *E. coli* strain JM109 and selected with 10 µg/ml of gentamicin. Plasmid DNA was isolated from the gentamicin resistant colonies. PCR was used to confirm the presence of the pBSV2G-*fliZ*$^+$ plasmid.

2.9 Inactivation of *bb0773*

The *bb0773* (425 bp) gene was inactivated using overlapping PCR as described for *fliZ* inactivation. Parts one, two, and three contain overlapping sequences. The final PCR product containing all three parts was ligated into pGEM®-T Easy Vector creating the Δ*bb0773*-Easy plasmid (Figure 14). Electroporation and platings were performed as described above into *B. burgdorferi* strain B31A. Genotyping of Δ*bb0773* was done using a primer that binds to the wild type, bb0773-P1F, and one that binds to the kanamycin cassette.

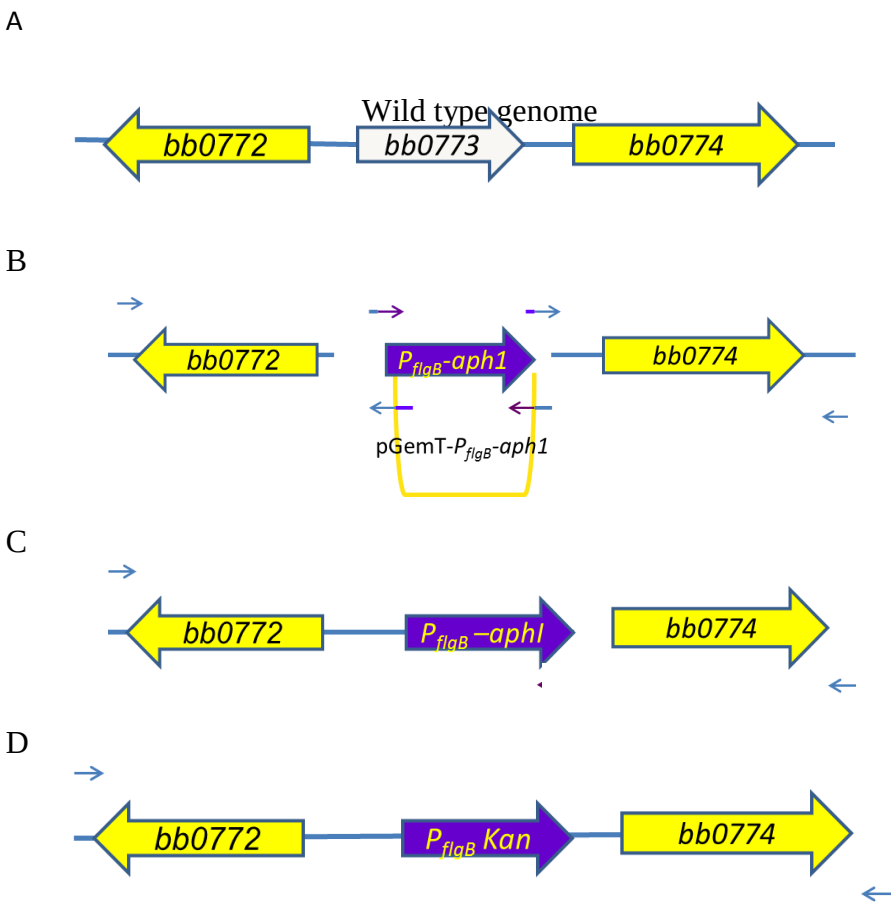

Figure 14. Schematic representation of the construction of Δ*bb0773* vehicle. A) Step 1: Amplify DNA fragments with paired primers. B) Join the first two fragments using overlapping PCR. C) Connect the third fragment to the first two using overlapping PCR for the completed product (D).

2.10 Western blotting

Sodium dodecyl sulfate polyacrylamide gel electrophoresis (SDS-PAGE) and Western blotting with an enhanced chemiluminescent detection method were carried out according to the manufacturer's instructions (GE Healthcare). A Bio-Rad Bradford assay was used to determine the relative concentration of proteins in the wild type and mutant cell lysates. Equal portions of

the lysates was loaded in each lane for SDS-PAGE, transferred to polyvinylidene fluoride membranes, and subjected to Western blotting using specific antibodies. Specific reactivities of the antibodies with *B. burgdorferi* proteins have been reported (74).

2.11 Microscopy and computer-assisted motion analysis

B. burgdorferi cells were observed using dark-field microscopy (Zeiss Axio Imager M1; Carl Zeiss Inc.) connected to an AxioCam digital camera to capture images. Cells were suspended in BSK-II buffer containing 1% 400 mesh methylcellulose (Sigma-Aldrich Co.) and recorded at room temperature. Cells were tracked using Axiovision software. For each strain, at least 15 individual cells were recorded for up to 30 seconds. Results are expressed as the total distance the center of each cell traveled/number of seconds the cell was tracked. The resulting velocity (μm/s) is a minimal velocity, as cells do not translate during flexes. The standard deviation of the results was calculated and compared using the Student's *t*-test. A $P = 0.05$ value is considered significant.

2.12 Cryo-electron tomography

Late log phase *B. burgdorferi* cells in a concentration of approximately 1×10^8/ml were centrifuged at 5,000 × *g* for 5 min in 1.5 ml tubes and the resulting pellet was rinsed gently with phosphate-buffed saline (PBS) prior to resuspension in 50 to 100 μl PBS for a final concentration of approximately 2×10^9 cells/ml (79). Aliquots of micron gold clusters were added to the resuspended viable *B. burgdorferi* cells in PBS as reference markers for image alignment (86). 4 μL of the cell samples were embedded in freshly glow-discharged holey carbon grids, flash frozen in liquid ethane and maintained at −180°C, using a homemade gravity-driven plunger

apparatus (79). The frozen samples were imaged at the temperature of liquid-nitrogen using a Polara electron microscope (FEI Company) equipped with a 4K × 4K charge-coupled-device camera (TVIPS; GMBH, Gauting, Germany) (79). Low-dose single-axis-tilt (with tilt angles of ± 65°) series were collected from each cell at −4 to −6 μm defocus with a cumulative dose of approximately 100 e−/Å2 spread over 131 images using the FEI "batch tomography" software program. . Using reference markers and the IMOD software package, consecutively tilted images were aligned with respect to each other (79, 86) . 3-D cryo-tomograms were reconstructed using weighted back-projection implemented in the software package Protomo after additional refinement using projection matching (46).

For 3-D classification and averaging, the positions and orientations of the flagellar motors in each tomogram were determined manually (79). A point was marked at each: the center of the basal body, the turning point of the hook, and a point on the flagellar filament for each flagella image (79). This provided the x, *y*, and *z* coordinates to determine the orientation of the flagellar motor and was used for an initial estimate of the alignment parameters, which were afterward refined iteratively (79).

A structure with 16-fold symmetry emerged after multiple cycles of alignment and averaging (79). To confirm this result, which was obtained by the alignment to a single reference, several cycles of a reference-free alignment procedure were applied (87). A single cycle of the procedure consisted of a classification step, in which the data set was separated into 20 classes (79). The class averages were then aligned with respect to each other and the alignment transformations of each class applied to the raw subvolumes of the respective members of the class, after which a new cycle was started (79).

Tomographic reconstructions were visualized by using IMOD (86). The 3-D segmentations of flagellar filaments, peptidoglycan, outer surface proteins, and outer and cytoplasmic membranes were manually constructed (74).

CHAPTER 3: RESULTS

3.1 Δ*cheY2* mutant and effects of chemotaxis on virulence.

Δ*cheY1* and Δ*cheY2* mutants were previously constructed in the high passage, avirulent strain, so their infection potential could not be evaluated. To perform a mouse and tick-mouse infection assays, we needed to make mutants in B31A3 strain that retains all virulence associated plasmids. As such, we constructed a plasmid to inactivate the genes by inserting an antibiotic resistance cassette within *cheY1* and *cheY2* separately. Since *cheY2* is located at the end of its operon, a polar effect on downstream genes expression is not expected. Accordingly, we inserted a P_{flgB}-*aph1* cassette within *cheY2* (81). This construct yielded *cheY2* mutants in the virulent strain of *B. burgdorferi* as confirmed by genotyping and a Western blot using CheY2 specific polyclonal antisera (Figure 15 and 16). A similar construct in *cheY1* has not yet yielded any mutants.

A

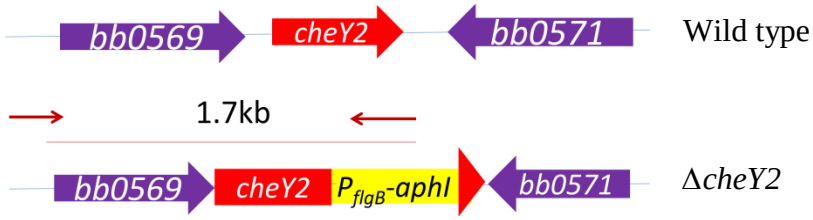

B

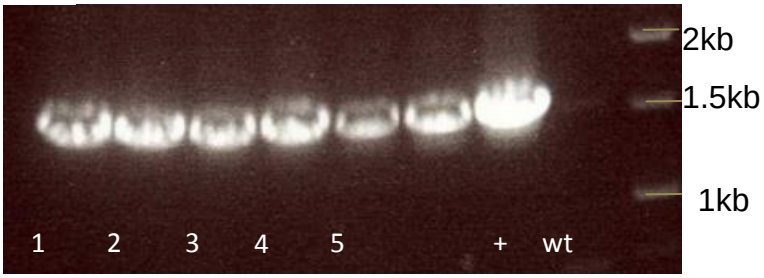

Figure 15. Genotyping of *cheY2* mutant. A) Diagram showing the location of the primer sites arrows used for genotyping. One primer binds to the P_{flgB}-*aphI* cassette and the other to the *cheY2* genomic DNA. Resulting PCR is expected to yield a 1574 bp band for the mutant and the positive control but no DNA band for wild type. B) Agarose gel displaying PCR results from *cheY2* mutants. Lanes 1 through 6 are mutants; lane 7 is the positive control, which is the *ΔcheY2*-Easy plasmid we used to construct the mutant. Lane 8 shows wild type *B. burgdorferi* genomic DNA which was used as a negative control. The DNA size marker is posted to the right.

Figure 16. Western blot of *cheY2* mutant. Equal amount of wild type and the mutant *B. burgdorferi* cell lysates was loaded in each lane for SDS-PAGE, transferred to polyvinylidene fluoride membranes, and subjected to Western blotting using anti *B. burgdorferi* CheY2 antibodies. A protein band (12 kD) was detected in the wild type but not in the mutant. As reported previously, this 12 kD band is CheY2.

3.2 Identification and characterization of a potential collar protein.

To find the genes encoding the collar structure, we first wanted to identify possible candidates. Rajagopala et al. provided a list of 176 motility protein interactions in *Treponema pallidum* that they created from known interactions from literature and from their own comprehensive array-based yeast-two-hybrid screens against *Campylobacter jejuni* (88). Additionally, more interactions were predicted based on interactions between other bacteria, such as *E. coli, B. subtilis, C. jejuni,* and *Helicobacter pylori.* These data was processed with the STRING database to further refine the list of possible interactions. In total, this involved 133 proteins in *T. pallidum,* many of which have unknown functions (88). The gene encoding the collar structure has not been identified in *T. pallidum* either, and since it also a spirochete, the list of unidentified motility genes is quite useful. From this list, we wanted to determine if we could find homologues in *B. burgdorferi*. We hypothesized that one of the proteins of unknown function could be a collar protein in *T. pallidum*. To narrow down the list of possible candidates, we removed the homologues that have already been characterized in *B. burgdorferi* and other spirochetes because they cannot be the collar structure. From the remaining genes, we further removed any genes that have homologues in non-spirochete species because the collar is unique to spirochetes. Additionally, based on cryo-ET data (Figure 16), the collar structure is located near the periplasmic flagellar motor (MotA and MotB), FliL, and situated on top of the MS-ring FliF proteins. This data served as a very good clue for us to look for any unidentified proteins that interacted with *T. pallidum* FliF, FliG, FliL, MotA or MotB. One *T. pallidum* gene that we focused on was *tp0708*. Rajagopala et al. indicated that this protein interacted with FlhA, FliG, FliF, and *T. pallidum's* homologue of *B. burgdorferi's* FlbB, a protein of unknown function in the flagellar (*flgB)* operon (89). All of these genes function in motility, or are hypothesized to do

so. FlhA, FliG-2, and FliF are known to localize close to the base of the basal body. Also, Tp0708 has homologues only in spirochetes, which is important, because the collar structure is found only in spirochetes. *bb0526* is the *B. burgdorferi* locus that shares highest similarity with Tp0708. These two proteins share an amino acid sequence identity of 28%. *bb0526* has not yet been characterized in any spirochetes. It appears to be the first gene in a bicistronic operon with *bb0527*. Bb0527 is a putative *baf* family transcriptional activator. There is no evidence that it plays any role in motility. Similar to all known motility and chemotaxis genes in *B. burgdorferi*, *bb0526* is located in the chromosome. Additionally, as can be seen in the cryo-ET images, the collar structure is likely inserted to the (inner) membrane and thus this protein(s) could possess a transmembrane domain. Based on these criteria, we predict that Bb0526 is a potential collar protein and may contribute to periplasmic flagellar assembly and motility.

Accordingly, we constructed mutants in *B. burgdorferi* avirulent and virulent backgrounds. Genotyping of the mutants was done with PCR amplification and gel electrophoresis (Figure 17). Our PCR results produced a 3.9 kb band for wild type and a 4.25 kb band for the mutant, as expected indicating we successfully isolated a *bb0526* mutant (Figure 17). After creating these mutants, we determined if the mutant exhibits a phenotype. We observed the cells under a dark-field microscope, noting a difference between the morphology of wild type cells and Δ*bb0526*. The Δ*bb0526* cells had a less pronounced wave-like morphology than the wild type (Figure 18). To determine *bb0526* mutant's motility phenotype, we performed methylcellulose assays using dark-field microscopy and cell tracking software. The methylcellulose assay revealed that the mutants had a significantly lower swimming velocity than the wild type cells (Figure 19).

A

B

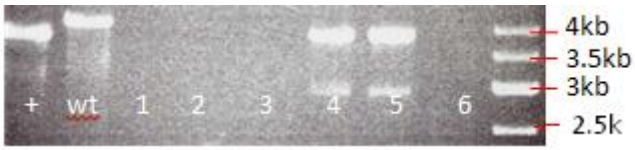

Figure 17. Genotyping of *bb0526* mutants. A) A diagram demonstrating the position of the primers. Shown here are the results for B31A3 background. Genotype results for B31A clones are not shown but are the same. B) Agarose gel of PCR results of clones 1-6. The positive control (+) is the plasmid we used to create the mutant and the wild type (wt) is *B. burgdorferi* genomic DNA. The expected size for the positive control and mutants is 3.90 kb and 4.25 kb for the wild type. Based on this agarose gel, lanes 4 and 5 are the expected *bb0526* mutants.

A

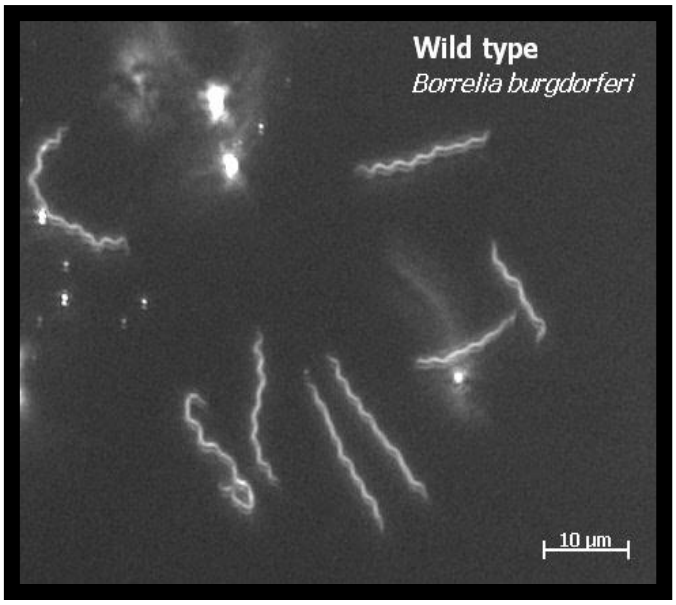

B

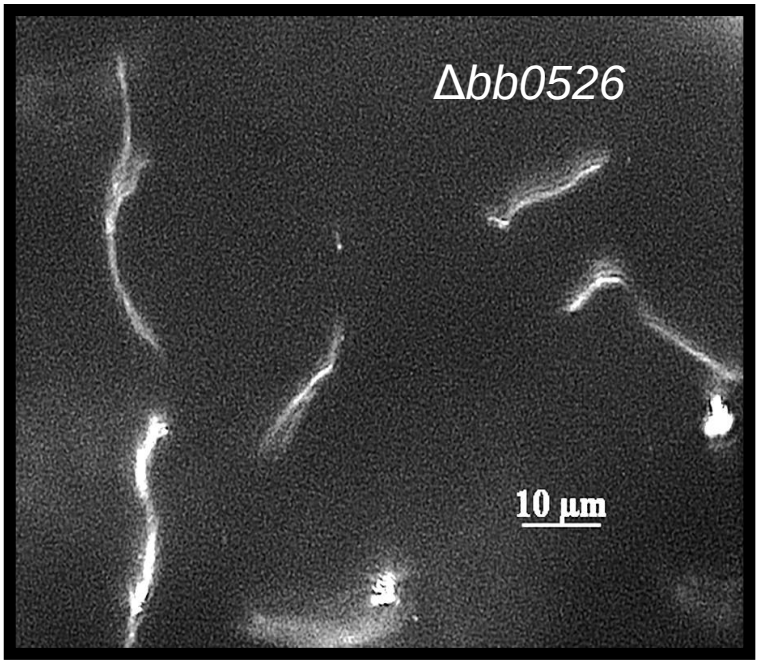

Figure 18. Dark-field microscopy image of Δ*bb0526* cells. A) Dark-field microscopy image of wild type cells. B) Dark-field microscopy image of Δ*bb0526* cells indicating drastic reduction of flat-wave morphology.

Additionally, when swimming, the mutant cells appeared slower and the movements of one pole of the cells was not coordinating with the other pole.

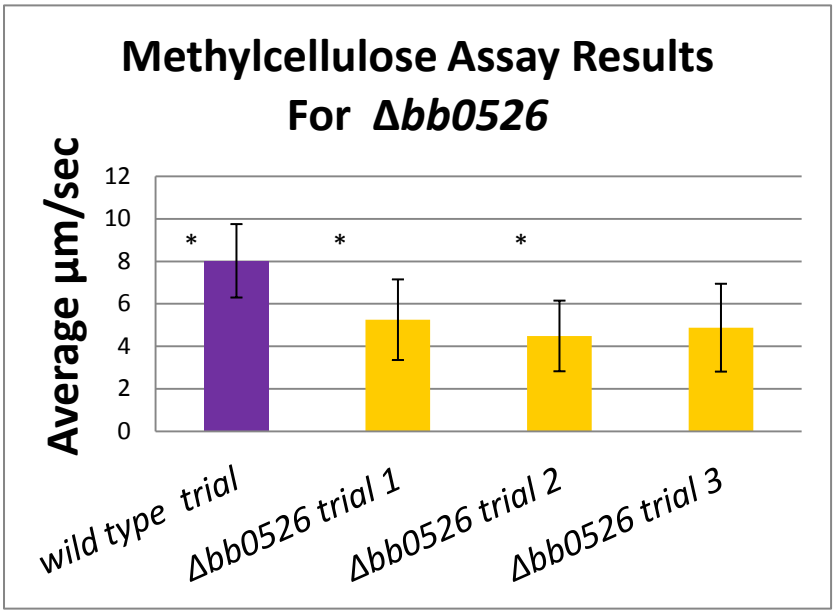

Figure 19. Methylcellulose assay results. This graph shows the results of three Δ*bb0526* methylcellulose trials in the B31A background. The asterisks represent statistically significant difference from wild type based on the Students *t*-test (P = 0.05).

3.3 bb0526 does not encode the collar structure, but may associate with it.

Simultaneously, we analyzed the mutants with cryo-electron tomography to pinpoint the defect caused by the inactivation of *bb0526.* The number of flagella did not differ from wild type (Table 1). Examination of the mutant cells poles at a molecular level using cryo-ET revealed that the outer membrane, inner membrane, and peptidoglycan layers are intact. The location of basal bodies and flagella are similar to wild type (Figure 20). An image of the side view of the Δ*bb0526* flagellar basal body also reveals no differences from wild type (Figure 21). However, a close up view of the top of the basal bodies reveals that an area of lower density in the Δ*bb0526* basal body around the area of the stator. The ruffling at the outer edge of the stator

appears to have less density in the Δ*bb0526* cells compared to the wild type, as can be seen in a computer aided model on Figure 21C,D,G,H. Because of its location, our cryo-ET data suggests that BB0526 provides a connection between the stator and the collar.

Cells	Number of periplasmic flagella per cell:	Sample Size:
Wild Type	9.3±1.3	21
Δ*bb0526*	9.4±1.6	25

Table 1. Inactivation of Δ*bb0526* did not produce significantly less periplasmic flagella. This table shows the flagella count per cell of the Δ*fliZ* and the wild type cells with the standard deviations indicated by the "±". Statistically significant deviation from wild type is indicated by an asterisks where P = 0.05. Data gathered by Jun Liu and Xiaowei Zhao from the University of Texas at Houston.

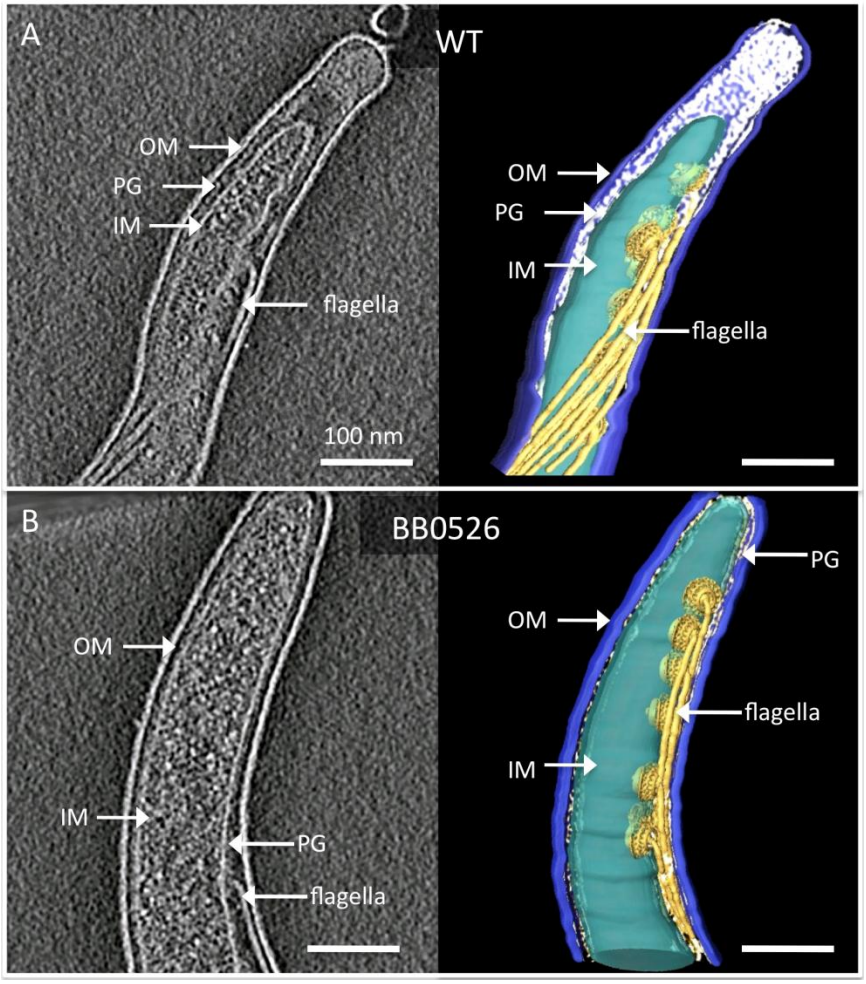

Figure 20. 3-D reconstruction of the cells of *B. burgdorferi* by cryo-electron tomography. (A) A Cryo-ET section (left panel) and surface rendering (right panel) from a wild type cell tomogram. (B) A Cryo-ET section (left panel) and surface rendering (right panel) from a Δ*bb0526* cell tomogram. OM: outer membrane; IM: inner membrane; PG: peptidoglycan. The OM (blue), IM (cyan), PG (white), and flagellar filament (yellow) were manually segmented by Amira. Averaged structures of the flagellar motors were computationally mapped back into their cellular context. Images created by Jun Liu and Xiaowei Zhao from the University of Texas at Houston.

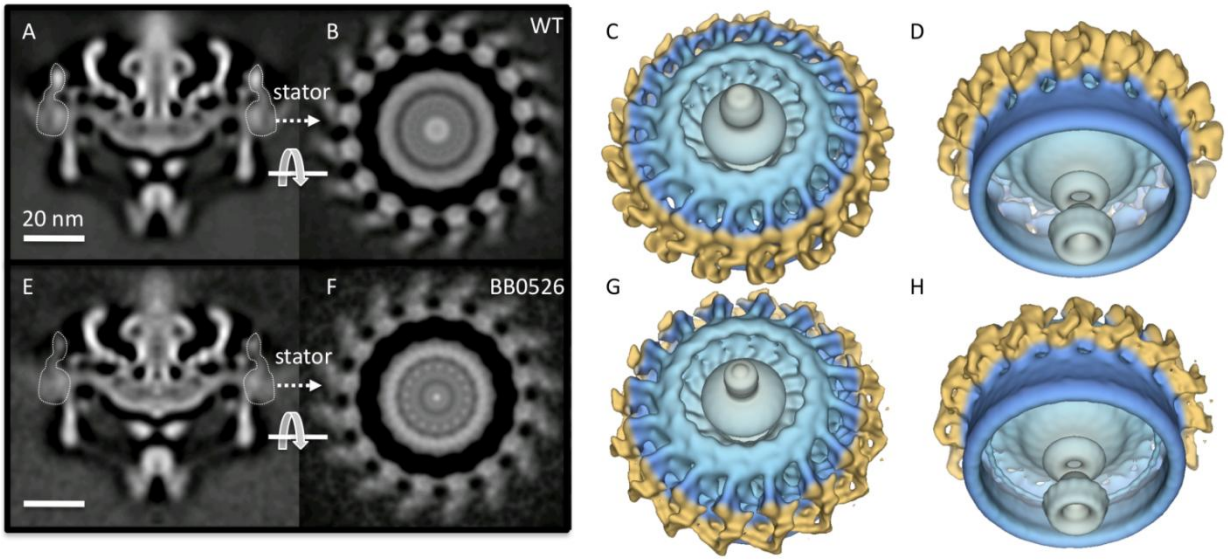

Figure 21. Averaged structures of the flagellar motors. (A) Side view of wild type flagellar motor. The densities of the stators were outlined from the density map. (B) Top view of the stators showing a ring-like structure composed of 16 particles. (C, D) Surface-rendering of the wild type flagellar motor of *B. burgdorferi*. (E-H) The flagellar motor of Δ*bb0526*. The averaged structure shows the densities of stator are not as strong as those in wild type. The differences in the flagellar motors of wild type and Δ*bb0526* are highlighted in yellow. Images created by Jun Liu and Xiaowei Zhao from the University of Texas at Houston.

3.4 *bb0773* is not required for wild type motility.

Since *bb0526* was found not to encode the main body of the collar structure, we identified *bb0773* as a possible candidate. *B. burgdorferi*'s *bb0773* is a 435 base pair gene annotated as a hypothetical gene. We selected *bb0773* because of its location in the genome exclusively. It is located in a cluster of several motility genes —*bb0772* encodes the P-ring; *bb774* encodes FlgG, the basal body rod protein, and *bb0775* encodes the rod locates near the P-ring (15). All three proteins are located near the collar structure thus we hypothesized that a neighboring gene such as *bb0773* likely encodes for the collar structure. *bb0773* appears to be monocistronic as it is separated from its neighboring genes on either side by more than 100 bp. To determine the role of Bb0773, we created mutants in this gene by overlapping PCR and genotyped it with PCR to confirm the mutation as shown in Figure 22 below. The mutant cells and the positive control (Δ*bb0773*-Easy) amplified a 2.1 kb product, while there was no band for the wild type as expected. To determine if *bb0773* mutant cells exhibit motility and morphology phenotypes we performed methylcellulose assays and dark-field microscopy, however, we have not detected any discernible defect in the mutant cells using these assays. All results indicated that this mutant has wild type motility and morphology. Cryo-ET imagery gave no indication of any defect either (data not shown). Based on our data, we conclude that *bb0773* has no observable phenotype with respect to motility, morphology, or motor structure using the conditions tested.

A

Wild type genome

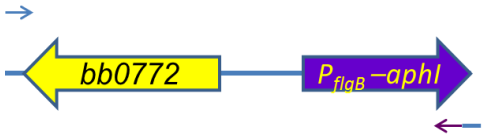

Δ*bb0773* genome

B

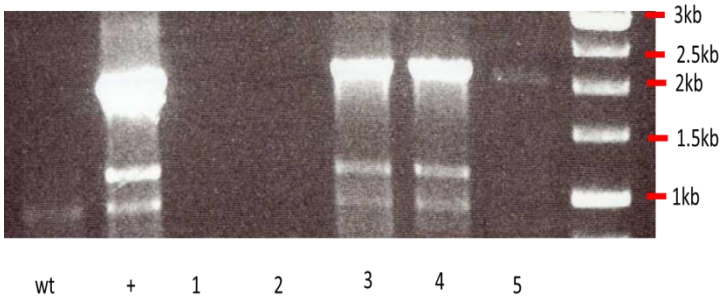

Figure 22. Genotyping of *bb0773* mutants. A) A diagram demonstrating the position of the primers. Shown here are the results for B31A background. B) Agarose gel of PCR results of clones 1-5. The positive control (+) is the plasmid we used to create the mutant and the wild type (wt) is *B. burgdorferi* genomic DNA. The expected size for the positive control and mutants is 2.1 kb and nothing is expected for the wild type.

3.5 Δ*fliZ* cells have a reduced flagella count.

In other bacteria such as *S. enterica*, inactivation of *fliO*, which is a *fliZ* homolog, resulted in mutant cells that are slower growing and less motile (83). Recently we have reported that non-motile *B. burgdorferi* mutants are unable to establish infection in mice through needle injection or tick bite. Additionally, the mutant spirochetes were unable to transmit from infected ticks to naive mice (19). If *B. burgdorferi's fliZ* is a true *fliO* homologue, we expect that the *fliZ* mutant cells will exhibit significantly decreased motility, this would allow us to test the hypothesis that *B. burgdorferi* requires full motility to be infective.

As mentioned before, we constructed a *fliZ* mutant plasmid using overlapping PCR to delete the *fliZ* by inserting a promoterless *aphI*. Being in the middle of a long operon, the in-frame insertion of a promoterless antibiotic resistance was reported to decrease the possibility of polar effects on downstream genes expression (90). Through homologous recombination, we used this plasmid to inactivate *fliZ* in *B. burgdorferi* B31A, and then we genotyped the transformants using PCR (Figure 23). Our PCR results produced a 1.72 kb band for the mutant and no band for the wild type, as expected indicating that we successfully isolated a *fliZ* mutant.

A

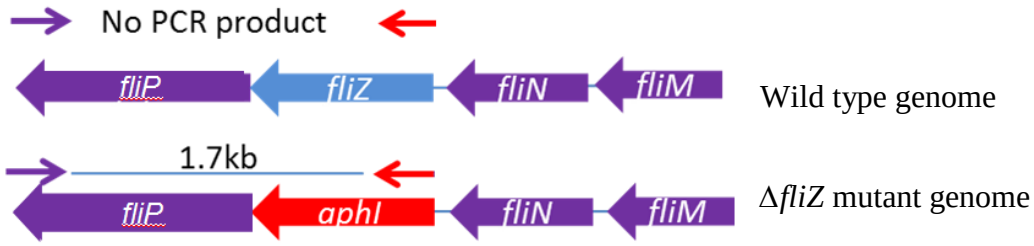

B

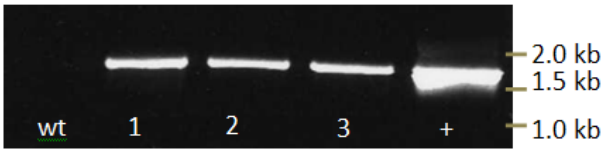

Figure 23. Genotyping of *fliZ* mutants. A) This diagram shows the primer binding sites (arrows). One primer will only bind to the kanamycin resistance cassette, *aphI*, which is why there is no band in the wild type lane. B) Agarose gel displaying PCR product with the expected size of 1.72 kb from the B31A Δ*fliZ* mutants. The lanes are labeled underneath the bands and the size of the DNA bands is posted to the right. The positive control in the last lane is the plasmid that we used to create the mutants.

After inactivation and confirmation of the mutant, we examined the morphology of the Δ*fliZ* mutant using dark-field microscopy. Δ*fliZ* cells displayed a similar morphology to the wild type, however the amplitude of the waves was noticeably decreased (Figure 24).

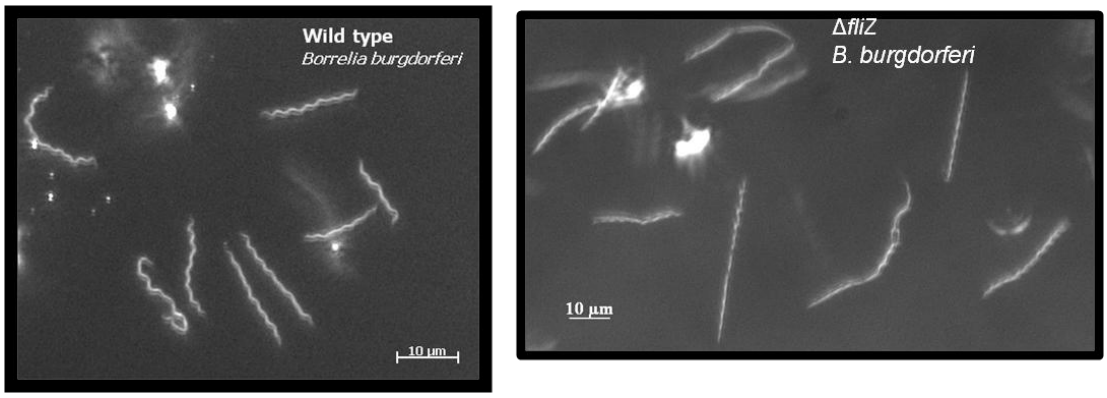

Figure 24. Dark-field microscopy of Δ*fliZ* cells. A) This image shows wild type cells for comparison. B) The Δ*fliZ* cells have a similar flat-wave morphology compared to the wild type cells; however, the amplitude of the waves is noticeably decreased in the Δ*fliZ* cells.

We also performed a methylcellulose assay to determine if the mutant had a motility phenotype. Unlike the *S. enterica fliO* mutants, the *B. burgdorferi fliZ* mutants had no significant motility defects from wild type cells, despite the apparent difference in morphology (Figure 25).

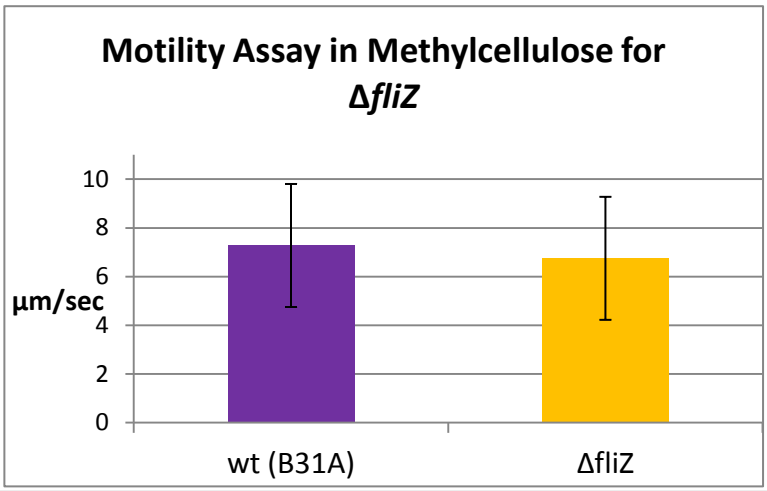

Figure 25. Methylcellulose assay indicates that *fliZ* mutant cells are not less motile than the wild type cells. This test was repeated three times (not shown) without a statistically significant difference from wild type based on the Students *t*-test (p=0.05).

Simultaneously, we analyzed the mutants with cryo-electron tomography to determine the morphology caused by the absence of *fliZ.* Cryo-ET revealed that the Δ*fliZ* mutants assemble flagella properly, in regards to the location and structures of the flagella and the flagella motors. However, the mutant cells synthesized and assembled less periplasmic flagella compared to wild type (Figure 26 and Table 2).

Cells	Number of periplasmic flagella per cell:	Sample Size:
Wild Type	9.3±1.3	21
Δ*fliZ* (trial 1)	7.5±1.5 *	18
Δ*fliZ* (trial 2)	6.5±1.8	17
Δ*fliZ* complement (trial 2)	10.2±2.6	9

Table 2. Inactivation of *fliZ* produced significantly less periplasmic flagella than wild type. Our complement restored the wild type phenotype. This table shows the flagella count per cell of the Δ*fliZ* and the wild type cells with the standard deviations indicated by the "±". Statistically significant deviation from wild type is indicated by an asterisks where p= 0.05. Data gathered by Jun Liu and Xiaowei Zhao from the University of Texas at Houston.

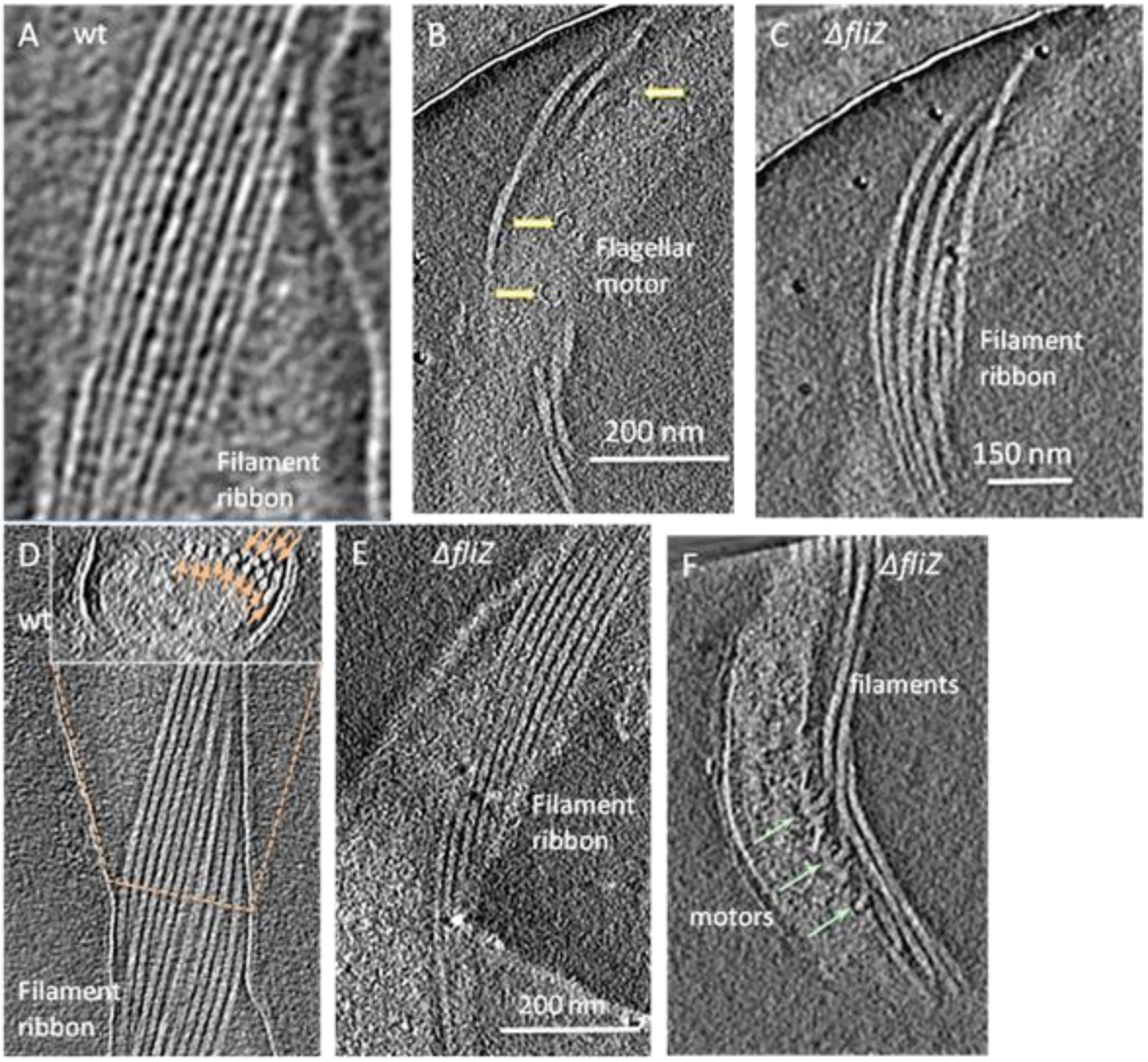

Figure 26. Cryo-ET results of Δ*fliZ* cells. A) This image shows the wild type flagella filament as it wraps around the cell cylinder. B) An image showing the Δ*fliZ* flagellar motors assembled at cell tip, where the flagella originate. C) Another image of the same cell showing the Δ*fliZ* flagellar filaments form a ribbon. D) Image of wild type cell. The inset panel shows the cross-section of the wild type cell cylinder. Filaments are stacked in the ribbon as indicated by the arrows. E) A section of the Δ*fliZ* core showing that the flagella are normally assembled in *fliZ*- cell. F) Image of Δ*fliZ* cell pole indicating proper location of flagella motors. Images created by Jun Liu and Xiaowei Zhao from the University of Texas at Houston.

To demonstrate that the *fliZ* mutant phenotype was due solely to the mutation and not due to a polar effects or a secondary alteration elsewhere, we complemented the mutant *in trans* using the pBSV2G-*fliZ*$^{+}$ plasmid (figure 27).

A

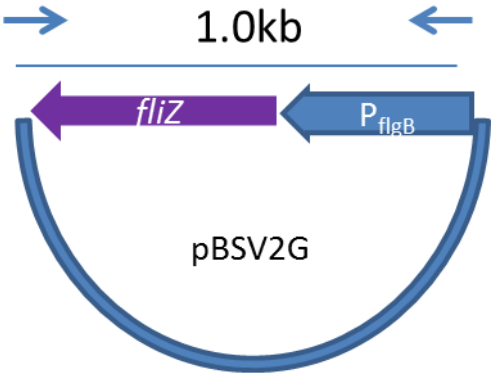

B

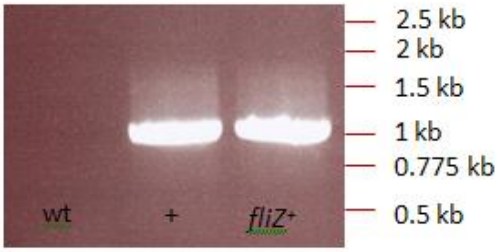

Figure 27. Results of plasmid rescue for *fliZ*$^{+}$cells. A) This diagram shows the primer binding sites (red arrows). One primer binds *fliZ* and the other primer binds to P_{flgB}, which is why there is no band in the wild type lane, for these fragments are too far apart from each other in the wild type genome.

B) Agarose gel displaying PCR product with the expected size of 1040 bp for the *fliZ*$^{+}$ cells. The lanes are labeled underneath the bands and a DNA size marker is posted to the right. The positive control in the middle lane is the plasmid that we used to create the mutant, pBSV2G-*fliZ*$^{+}$.

The complemented cells were analyzed with cryo-ET to determine the restoration of the normal numbers of periplasmic flagella. Our data indicate that the complemented *fliZ*$^{+}$ cells had a restored flagella number compared to the wild type (Table 2). Overall, our results indicate that unlike *S. enterica*, *B. burgdorferi* FliZ is crucial for controlling the flagellar number.

CHAPTER 4: DISCUSSION

4.1 *cheY1* and *cheY2*

The role of chemotaxis in establishing infection has been studied in many bacterial pathogens. *Helicobactor pylori*, for example, requires chemotaxis to navigate to the mucosal membrane of the stomach wall (91). Another bacterium, *Campylobacter jejuni*, has been shown to require chemotaxis in order to establish an infection (91). Through the inactivation of *cheA2*, Sze et al. have shown *B. burgdorferi* also requires chemotaxis for establishment of infection (17). One way to achieve a nonchemotactic mutant is to inactivate the *cheY* genes. Inactivation of the *cheY* gene in *E. coli* leads to loss of chemotactic ability (58). In *B. burgdorferi*, inactivation of *cheY3* leads to nonchemotactic mutants (63). Our unpublished results indicate that *cheY3* mutant spirochetes are unable to establish infection in C3H/HeN mice. Additionally, although Δ*cheY3* cells are able to survive in ticks, those mutant cells are unable to transmit from the infected ticks to naïve mice. Our results and data concur with Sze et al. and clearly demonstrate the importance of chemotaxis *in vivo* for *B. burgdorferi.*

B. burgdorferi, however, has three copies of the *cheY* gene (15, 71)(71)(71). Mutants in *cheY1* and *cheY2* have been shown to be chemotactic *in vitro* (63), thus their inactivation seemed to have no effect. We can say, however, that the growing *B. burgdorferi* cells actively transcribe and translate *cheY1* and *cheY2*, so they are not pseudogenes (71). We hypothesize that these genes are only necessary at certain phases of the spirochete's lifecycle. For example, one of the genes in question may be activated while *B. burgdorferi* is entering the tick and the other may be activated while exiting the tick or both genes are important for the tick-phase (acquisition and transmission or survivability in tick vector) of the spirochete's enzootic cycle. In order to

investigate the roles of CheY1 and CheY2 during the infectious life cycle of *B. burgdorferi*, we proposed to inactivate these genes in a virulent strain of *B. burgdorferi.* So far, we have succeeded in making a *cheY2* mutant in the virulent background that retained all endogenous plasmids required for virulence. In contrast to our progress with *cheY2*, we have not been able to achieve any mutants in the virulent background with *cheY1*. Genetic manipulations in *B. burgdorferi* are extremely difficult and it is not unusual to take multiple attempts in order to construct a mutant strain in the virulent background (19, 92). While not completed, these mutants would make an excellent specimen for investigating the link between virulence and chemotaxis. Preliminary data by Lin et al. indicates that *cheY2* mutants are noninfectious in mice, demonstrating that while *cheY2* may appear to be unnecessary for chemotaxis *in vitro*, it is required for survival in experimental mice (75). Our *cheY1* and *cheY2* mutants would afford an opportunity to investigate further the function of chemotaxis in the future.

4.2 *bb0526*

The collar structure is one of the largest structures featured in cryo-ET images of *B. burgdorferi's* periplasmic flagellar motors. For this reason, we hypothesized that the collar structure plays a central role in the assembly or provide support to the flagella for efficient motility function. We have determined that the *B. burgdorferi bb0526* mutant has a swimming defect despite the possession of normal number of periplasmic flagella. While it was not possible to discern the cause of the motility defect by dark-field microscopy we took advantage of cryo-ET that can detect individual flagellar structures at a molecular level. We found that densities corresponding to a flagellar structure are missing near the base of the collar where the structure connects with the motor stator (MotA and MotB) suggesting that BB0526 corresponds to the base of the collar or is part of the collar structure. The flagellum is a complex molecular

machine with each protein in a very precise place. Our evidence indicates that BB0526 connects the collar structure to the stator and without this connection and support, the collar may be unable to provide the necessary support to the motors which resulted in decreased motility phenotype. In order to confirm the hypothesis that BB0526 connects or binds the stator we plan to study protein-protein interactions between BB0526 and stator (MotA and MotB).

Our laboratory has reported that non-motile *flaB* mutants are unable to infect mice through needle injection or tick bites (19). However, an incrementally reduced motility mutant has not been evaluated in the infectious life cycle of *B. burgdorferi*. We posit that *bb0526* mutant is a good candidate for determining whether *B. burgdorferi* can still be infectious with limited motility. We hypothesize that Δ*bb0526* cells will be significantly less infectious than the wild type in mice. If this turns out to be true, it will indicate that full motility is crucial for outsmarting host immune responses and establishment of infection. Additionally, we hypothesize that the less motile *bb0526* mutant will be unable or have limited ability to be acquired and/or transmitted by the tick in tick-mouse-tick cycle infections. Previously we have reported that motility is important for *B. burgdorferi*'s intimate binding to the tick midguts and consequently, this binding provide survivability of the spirochetes in ticks (19). Since *bb0526* is **not** a non-motile mutant, we predict that *bb0526* will be able to survive in fed ticks, but may not be able to transmit the infection to naïve mice. We hypothesize that this defect will limit its ability to invade tissues within a host.

4.3 *bb0773*

Our results reveal no motility or chemotactic functions for *bb0773.* There may, however, be other functions for this gene that are not related to motility or chemotaxis. We will keep an open mind with this gene and explore its possibilities, should they arise in the future.

4.4 *fliZ*

In other bacteria inactivation of *fliZ* leads to slow growth and motility defects (83). The aim of our research was to determine if inactivation of *fliZ* would create a similar slow mutant in *B. burgdorferi,* which would give us an opportunity to demonstrate the role of motility in infection. After inactivating *fliZ,* we discovered a mutant with reduced number of periplasmic flagella, but we did not notice a motility defect. However, this result could be due to a lack of sensitivity in our methods. If a lack of sensitivity is not a problem, we assume that FliZ is a protein that is involved in regulating the number of periplasmic flagella. The restoration of the wild type phenotype through complementation supports our hypothesis that *fliZ* was the cause of this reduction in flagella.

FlhF and FlhG are known regulators of the flagella numbers in *Vibrio spp.* (*V. cholera* and *V. alginolyticus*) (93-95) and *C. jejuni (96),* however, there is no evidence that *fliZ* associates with these well-known regulators. *B. burgdorferi* possesses a homolog of FlhF and FlhG (15). Although not known, it is possible that FliZ interacts with these proteins in order to control the number of periplasmic flagella or FliZ may act alone to control the flagellar number in the spirochetes. Alternatively, we believe the cause of the reduced numbers of periplasmic flagella is a result of the lack of stability in FliP, a protein that FliZ regulates in other bacteria (83). FliP is a known flagellar protein that is involved in exporting flagella using type-III secretion system (83).

We were surprised that we could not detect a motility defect, despite the reduced number of periplasmic flagella in the *fliZ* mutant cells using the bacterial tracking software. We will perform swarm plate motility assays that require extended period of incubation for the cells to swarm out from the initial site of inoculation in the soft-agarose plate. If, by swarm plate assay, we find that the *fliZ* mutant exhibits reduced motility due to possessing less periplasmic flagella, it will be intriguing to determine whether or not *B. burgdorferi* needs full motility to be infectious in its natural lifecycle. While we are in a good position to determine if full motility is important for the infectious life cycle of *B. burgdorferi* using *bb0526* and *fliZ* mutants, it is important to note that these two mutants are different. While *bb0526* exhibits a reduced motility phenotype due to inefficient interactions between the stator and collar, the *fliZ* mutant cells possess less periplasmic flagella. We have laid the groundwork for such an experiment in the future.

REFERENCES

1. Kaslow RA. New england's own arthritis? JAMA: The Journal of the American Medical Association. 1977;238(4):330-1.

2. Hazard GW, Leland K, Mathewson HO. *Erythema chronicum migrans* and " Lyme arthritis". JAMA: the journal of the American Medical Association. 1976;236(21):2392-.

3. Steere AC, Malawista SE, Hardin JA, Ruddy S, Askenase W, Andiman WA. *Erythema chronicum migrans* and Lyme arthritis. the enlarging clinical spectrum. Ann Intern Med. 1977;86(6):685.

4. Burgdorfer W, Barbour AG, Hayes SF, Benach JL, Grunwaldt E, Davis JP. Lyme disease-a tick-borne spirochetosis? Science (New York, NY). 1982;216(4552):1317.

5. Johnson RC, Schmid GP, Hyde FW, Steigerwalt A, Brenner DJ. *Borrelia burgdorferi* sp. nov.: Etiologic agent of Lyme disease. Int J Syst Bacteriol. 1984;34(4):496-7.

6. Bacon RM, Kugeler KJ, Mead PS. Surveillance for Lyme disease--United States, 1992-2006. Department of Health & Human Services, Centers for Disease Control and Prevention; 2008.

7. Clinical manifestations of confirmed Lyme disease cases--United States, 2001-2010 [Internet]. 1600 Clifton Rd. Atlanta, GA 30333, USA: Centers for Disease Control and Prevention National Center for Emerging and Zoonotic Infectious Diseases (NCEZID) Division of Vector-Borne Diseases (DVBD); 2012 [updated April 13, 2012; cited April 1, 2013]. Available from: http://www.cdc.gov/ Lyme/stats/chartstables/casesbysymptom.html.

8. Preac-Mursic V, Wilske B, Reinhardt S. Culture of *Borrelia burgdorferi* on six solid media. European Journal of Clinical Microbiology & Infectious Diseases. 1991;10(12):1076-9.

9. Purser JE, Norris SJ. Correlation between plasmid content and infectivity in *borrelia burgdorferi* . Proceedings of the National Academy of Sciences. 2000;97(25):13865-70.

10. Lawrenz MB, Kawabata H, Purser JE, Norris SJ. Decreased electroporation efficiency in *Borrelia burgdorferi* containing linear plasmids lp25 and lp56: Impact on transformation of infectious *B. burgdorferi* . Infect Immun. 2002;70(9):4798-804.

11. Labandeira-Rey M, Skare JT. Decreased infectivity in *Borrelia burgdorferi* strain B31 is associated with loss of linear plasmid 25 or 28-1. Infect Immun. 2001;69(1):446-55.

12. Casjens S, Palmer N, Van Vugt R, Mun Huang W, Stevenson B, Rosa P, et al. A bacterial genome in flux: The twelve linear and nine circular extrachromosomal DNAs in an infectious

isolate of the Lyme disease spirochete *Borrelia burgdorferi* . Mol Microbiol. 2002;35(3):490-516.

13. Barbour AG. Isolation and cultivation of Lyme disease spirochetes. Yale J Biol Med. 1984;57(4):521.

14. Charon NW, Goldstein SF. Genetics of motility and chemotaxis of a fascinating group of bacteria: The spirochetes. Annu Rev Genet. 2002;36(1):47-73.

15. Fraser CM, Casjens S, Huang WM, Sutton GG, Clayton R, Lathigra R, et al. Genomic sequence of a Lyme disease spirochaete, *borrelia burgdorferi*. Nature. 1997;390(6660):580-6.

16. Radolf JD, Caimano MJ, Stevenson B, Hu LT. Of ticks, mice and men: Understanding the dual-host lifestyle of Lyme disease spirochaetes. Nature Reviews Microbiology. 2012;10(2):87-99.

17. Sze CW, Zhang K, Kariu T, Pal U, Li C. *Borrelia burgdorferi* needs chemotaxis to establish infection in mammals and to accomplish its enzootic cycle. Infect Immun. 2012;80(7):2485-92.

18. Li C, Xu H, Zhang K, Liang FT. Inactivation of a putative flagellar motor switch protein FliG1 prevents *Borrelia burgdorferi* from swimming in highly viscous media and blocks its infectivity. Mol Microbiol. 2010;75(6):1563-76.

19. Sultan SZ, Manne A, Stewart PE, Bestor A, Rosa PA, Charon NW, et al. Motility is crucial for the infectious life cycle of *Borrelia burgdorferi*. Infect Immun. 2013.

20. Nau R, Christen H, Eiffert H. Lyme disease—current state of knowledge. Deutsches Arzteblatt International. 2009;106(5):72.

21. Orloski KA, Hayes EB, Campbell GL, Dennis DT. Surveillance for Lyme disease—United States, 1992–1998. MMWR CDC Surveill Summ. 2000;49(3):1-11.

22. Steere AC, Bartenhagen NH, Craft JE, Hutchinson GJ, Newman JH, Rahn DW, et al. The early clinical manifestations of Lyme disease. Ann Intern Med. 1983;99(1):76.

23. Steere AC, Sikand VK. The presenting manifestations of Lyme disease and the outcomes of treatment. N Engl J Med. 2003;348(24):2472-4.

24. Gota CE, Calabrese LH. Diagnosis and treatment of cutaneous leukocytoclastic vasculitis. International Journal of Clinical Rheumatology. 2013;8(1):49-60.

25. Duray PH. Clinical pathologic correlations of Lyme disease. Review of Infectious Diseases. 1989;11(Supplement 6):S1487-93.

26. Steere AC, Batsford WP, Weinberg M, Alexander J, Berger HJ, Wolfson S, et al. Lyme carditis: Cardiac abnormalities of Lyme disease. Ann Intern Med. 1980;93(1):8.

27. Cary N, Fox B, Wright D, Cutler S, Shapiro L, Grace A. Fatal Lyme carditis and endodermal heterotopia of the atrioventricular node. Postgrad Med J. 1990;66(772):134-6.

28. Steere AC, Schoen RT, Taylor E. The clinical evolution of Lyme arthritis. Ann Intern Med. 1987;107(5):725-31.

29. Tory HO, Zurakowski D, Sundel RP. Outcomes of children treated for Lyme arthritis: Results of a large pediatric cohort. J Rheumatol. 2010;37(5):1049-55.

30. Steere AC, Klitz W, Drouin EE, Falk BA, Kwok WW, Nepom GT, et al. Antibiotic-refractory Lyme arthritis is associated with HLA-DR molecules that bind a *Borrelia burgdorferi* peptide. J Exp Med. 2006;203(4):961-71.

31. Steere AC, Hutchinson GJ, Rahn DW, Sigal LH, Craft JE, Desanna ET, et al. Treatment of the early manifestations of Lyme disease. Ann Intern Med. 1983;99(1):22.

32. Lyme disease data [internet] [Internet].; 2012. Available from: http://www.cdc.gov/Lyme/stats/index.html.

33. Schwan TG, Piesman J. Temporal changes in outer surface proteins A and C of the Lyme disease-associated spirochete,*Borrelia burgdorferi*, during the chain of infection in ticks and mice. J Clin Microbiol. 2000;38(1):382-8.

34. Coughlin RT, Fish D, Mather TN, Ma J, Pavia C, Bulger P. Protection of dogs from Lyme disease with a vaccine containing outer surface protein (osp) A, OspB, and the saponin adjuvant QS21. J Infect Dis. 1995;171(4):1049-52.

35. Kurtenbach K, De Michelis S, Etti S, Schäfer SM, Sewell H, Brade V, et al. Host association of *Borrelia burgdorferi* sensu lato–the key role of host complement. Trends Microbiol. 2002;10(2):74-9.

36. Lane RS, Loye JE. Lyme disease in California: Interrelationship of *Ixodes pacificus* (acari: Ixodidae), the western fence lizard (*Sceloporus occidentalis*), and *Borrelia burgdorferi* . J Med Entomol. 1989;26(4):272-8.

37. Gern L, Estrada-Pena A, Frandsen F, Gray J, Jaenson T, Jongejan F, et al. European reservoir hosts of *Borrelia burgdorferi* sensu lato. Zentralblatt für Bakteriologie. 1998;287(3):196-204.

38. Anderson JF. Epizootiology of *Borrelia* in *Ixodes* tick vectors and reservoir hosts. Review of Infectious Diseases. 1989;11(Supplement 6):S1451-9.

39. Padgett KA, Lane RS. Life cycle of *Ixodes pacificus* (acari: Ixodidae): Timing of developmental processes under field and laboratory conditions. J Med Entomol. 2001;38(5):684-93.

40. Schoeler GB, Lane RS. Efficiency of transovarial transmission of the Lyme disease spirochete, *Borrelia burgdorferi*, in the western blacklegged tick, *Ixodes pacificus* (acari: Ixodidae). J Med Entomol. 1993;30(1):80-6.

41. Donahue JG, Piesman J, Spielman A. Reservoir competence of white-footed mice for Lyme disease spirochetes. Am J Trop Med Hyg. 1987;36(1):92.

42. Brown RN, Lane RS. Lyme disease in california: A novel enzootic transmission cycle of *Borrelia burgdorferi* . Science (New York, NY). 1992;256(5062):1439.

43. Yuval B, Spielman A. Duration and regulation of the developmental cycle of *Ixodes dammini* (acari: Ixodidae). J Med Entomol. 1990;27(2):196-201.

44. DePamphilis M, Adler J. Fine structure and isolation of the hook-basal body complex of flagella from *Escherichia coli* and *Bacillus subtilis* . J Bacteriol. 1971;105(1):384-95.

45. Larsen SH, Reader RW, Kort EN, Tso W, Adler J. Change in direction of flagellar rotation is the basis of the chemotactic response in *Escherichia coli* . . 1974.

46. Turner L, Ryu WS, Berg HC. Real-time imaging of fluorescent flagellar filaments. J Bacteriol. 2000;182(10):2793-801.

47. Charon NW, Goldstein SF, Marko M, Hsieh C, Gebhardt LL, Motaleb MA, et al. The flat-ribbon configuration of the periplasmic flagella of *Borrelia burgdorferi* and its relationship to motility and morphology. J Bacteriol. 2009;191(2):600-7.

48. Motaleb MA, Corum L, Bono JL, Elias AF, Rosa P, Samuels DS, et al. *Borrelia burgdorferi* periplasmic flagella have both skeletal and motility functions. Proceedings of the National Academy of Sciences. 2000;97(20):10899-904.

49. Motaleb M, Sal MS, Charon NW. The decrease in FlaA observed in a *flaB* mutant of *Borrelia burgdorferi* occurs posttranscriptionally. J Bacteriol. 2004;186(12):3703-11.

50. Goldstein SF, Charon NW, Kreiling JA. *Borrelia burgdorferi* swims with a planar waveform similar to that of eukaryotic flagella. Proceedings of the National Academy of Sciences. 1994;91(8):3433-7.

51. Shi W, Yang Z, Geng Y, Wolinsky LE, Lovett MA. Chemotaxis in *Borrelia burgdorferi* . J Bacteriol. 1998;180(2):231-5.

52. Adler J. Chemotaxis in bacteria. Science (New York, NY). 1966;153(737):708.

53. Kort EN, Goy MF, Larsen SH, Adler J. Methylation of a membrane protein involved in bacterial chemotaxis. Proceedings of the National Academy of Sciences. 1975;72(10):3939-43.

54. Kondoh H, Ball CB, Adler J. Identification of a methyl-accepting chemotaxis protein for the ribose and galactose chemoreceptors of *Escherichia coli* . Proceedings of the National Academy of Sciences. 1979;76(1):260-4.

55. Williams SB, Stewart V. MicroReview: Functional similarities among two-component sensors and methyl-accepting chemotaxis proteins suggest a role for linker region amphipathic helices in transmembrane signal transduction. Mol Microbiol. 2002;33(6):1093-102.

56. Bilwes AM, Alex LA, Crane BR, Simon MI. Structure of CheA, a signal-transducing histidine kinase. Cell. 1999;96(1):131-41.

57. Gegner JA, Graham DR, Roth AF, Dahlquist FW. Assembly of an MCP receptor, CheW, and kinase CheA complex in the bacterial chemotaxis signal transduction pathway. Cell. 1992;70(6):975-82.

58. Parkinson JS, Houts SE. Isolation and behavior of *Escherichia coli* deletion mutants lacking chemotaxis functions. J Bacteriol. 1982;151(1):106-13.

59. Li J, Swanson RV, Simon MI, Weis RM. Response regulators CheB and CheY exhibit competitive binding to the kinase CheA. Biochemistry (N Y). 1995;34(45):14626-36.

60. Li C, Bakker RG, Motaleb MA, Sartakova ML, Cabello FC, Charon NW. Asymmetrical flagellar rotation in *Borrelia burgdorferi* nonchemotactic mutants. Proceedings of the National Academy of Sciences. 2002;99(9):6169-74.

61. Bren A, Eisenbach M. The N terminus of the flagellar switch protein, FliM, is the binding domain for the chemotactic response regulator, CheY. J Mol Biol. 1998;278(3):507-14.

62. McEvoy MM, Bren A, Eisenbach M, Dahlquist FW. Identification of the binding interfaces on CheY for two of its targets the phosphatase CheZ and the flagellar switch protein FliM. J Mol Biol. 1999;289(5):1423-33.

63. Springer WR, Koshland D. Identification of a protein methyltransferase as the cheR gene product in the bacterial sensing system. Proceedings of the National Academy of Sciences. 1977;74(2):533-7.

64. Stock JB, Koshland D. A protein methylesterase involved in bacterial sensing. Proceedings of the National Academy of Sciences. 1978;75(8):3659-63.

65. Trueba G, Old I, Saint Girons I, Johnson R. A*cheA cheW*operon in *Borrelia burgdorferi*, the agent of Lyme disease. Res Microbiol. 1997;148(3):191-200.

66. Motaleb M, Miller MR, Li C, Bakker RG, Goldstein SF, Silversmith RE, et al. CheX is a phosphorylated CheY phosphatase essential for *Borrelia burgdorferi* chemotaxis. J Bacteriol. 2005;187(23):7963-9.

67. Altschul, S. Gish, W. Miller, W. Myers, E. Lipman, D. Basic local alignment search tool. J Mol Biol. 1990(215: 403-410.):http://blast.ncbi.nlm.nih.gov/Blast.cgi.

68. Xu H, Raddi G, Liu J, Charon NW, Li C. Chemoreceptors and flagellar motors are subterminally located in close proximity at the two cell poles in spirochetes. J Bacteriol. 2011;193(10):2652-6.

69. Gassmann GS, Jacobs E, Deutzmann R, Göbel U. Analysis of the*Borrelia burgdorferi*GeHo fla gene and antigenic characterization of its gene product. J Bacteriol. 1991;173(4):1452-9.

70. Zhang K, Liu J, Tu Y, Xu H, Charon NW, Li C. Two CheW coupling proteins are essential in a chemosensory pathway of *Borrelia burgdorferi*. Mol Microbiol. 2012.

71. Motaleb MA, Sultan SZ, Miller MR, Li C, Charon NW. CheY3 of *borrelia burgdorferi* is the key response regulator essential for chemotaxis and forms a long-lived phosphorylated intermediate. J Bacteriol. 2011;193(13):3332-41.

72. Purine-binding chemotaxis protein *[Escherichia coli* str. K-12 substr. MG1655] [Internet].: ncbi.nlm.nih.gov; 2012 [updated 11 Jan. 2012; cited Feb. 14, 2013]. Available from: http://www.ncbi.nlm.nih.gov/protein/16129839.

73. Chemotaxis protein CheW [*Borrelia burgdorferi* B31] [Internet]. Nature: ncbi.nlm.nih.gov; 2012 [updated 27 Sep. 2012; cited 14 Feb. 2013]. Available from: http://www.ncbi.nlm.nih.gov/protein/15595015.

74. Motaleb MA, Pitzer JE, Sultan SZ, Liu J. A novel gene inactivation system reveals altered periplasmic flagellar orientation in a *Borrelia burgdorferi* fliL mutant. J Bacteriol. 2011;193(13):3324-31.

75. Lin T, Gao L, Zhang C, Odeh E, Jacobs MB, Coutte L, et al. Analysis of an ordered, comprehensive STM mutant library in infectious borrelia burgdorferi: Insights into the genes required for mouse infectivity. PloS one. 2012;7(10):e47532.

76. Kim EA, Price-Carter M, Carlquist WC, Blair DF. Membrane segment organization in the stator complex of the flagellar motor: Implications for proton flow and proton-induced conformational change†. Biochemistry (N Y). 2008;47(43):11332-9.

77. Kudryashev M, Cyrklaff M, Wallich R, Baumeister W, Frischknecht F. Distinct*in situ* structures of the *Borrelia* flagellar motor. J Struct Biol. 2010;169(1):54-61.

78. Sal MS, Li C, Motalab M, Shibata S, Aizawa S, Charon NW. *Borrelia burgdorferi* uniquely regulates its motility genes and has an intricate flagellar hook-basal body structure. J Bacteriol. 2008;190(6):1912-21.

79. Liu J, Lin T, Botkin DJ, McCrum E, Winkler H, Norris SJ. Intact flagellar motor of *Borrelia burgdorferi* revealed by cryo-electron tomography: Evidence for stator ring curvature and rotor/C-ring assembly flexion. J Bacteriol. 2009;191(16):5026-36.

80. Charon NW, Cockburn A, Li C, Liu J, Miller KA, Miller MR, et al. The unique paradigm of spirochete motility and chemotaxis. Annu Rev Microbiol. 2012;66(1).

81. Ge Y, Old IG, Saint Girons I, Charon NW. Molecular characterization of a large *Borrelia burgdorferi* motility operon which is initiated by a consensus sigma70 promoter. J Bacteriol. 1997;179(7):2289-99.

82. Ohnishi K, Fan F, Schoenhals GJ, Kihara M, Macnab RM. The FliO, FliP, FliQ, and FliR proteins of *Salmonella typhimurium*: Putative components for flagellar assembly. J Bacteriol. 1997;179(19):6092-9.

83. Barker CS, Meshcheryakova IV, Kostyukova AS, Samatey FA. FliO regulation of FliP in the formation of the *Salmonella enterica* flagellum. PLoS genetics. 2010;6(9):e1001143.

84. Motaleb MA, Miller MR, Bakker RG, Li C, Charon NW. Isolation and characterization of chemotaxis mutants of the Lyme disease Spirochete *Borrelia burgdorferi* using allelic exchange mutagenesis, flow cytometry, and cell tracking. Meth Enzymol. 2007;422:419-37.

85. Sartakova ML, Dobrikova EY, Terekhova DA, Devis R, Bugrysheva JV, Morozova OV, et al. Novel antibiotic-resistance markers in pGK12-derived vectors for *Borrelia burgdorferi* . Gene. 2003;303:131-7.

86. Kremer JR, Mastronarde DN, McIntosh JR. Computer visualization of three-dimensional image data using IMOD. J Struct Biol. 1996;116(1):71-6.

87. Winkler H, Zhu P, Liu J, Ye F, Roux KH, Taylor KA. Tomographic subvolume alignment and subvolume classification applied to myosin V and SIV envelope spikes. J Struct Biol. 2009;165(2):64-77.

88. Rajagopala SV, Titz B, Goll J, Parrish JR, Wohlbold K, McKevitt MT, et al. The protein network of bacterial motility. Molecular systems biology. 2007;3(1).

89. Ge Y, Charon NW. Identification of a large motility operon in*Borrelia burgdorferi*by semi-random PCR chromosome walking. Gene. 1997;189(2):195-201.

90. Sultan SZ, Pitzer JE, Miller MR, Motaleb MA. Analysis of a *Borrelia burgdorferi* phosphodiesterase demonstrates a role for cyclic-di-guanosine monophosphate in motility and virulence. Mol Microbiol. 2010;77(1):128-42.

91. Croxen MA, Sisson G, Melano R, Hoffman PS. The*Helicobacter pylori*chemotaxis receptor TlpB (HP0103) is required for pH taxis and for colonization of the gastric mucosa. J Bacteriol. 2006;188(7):2656-65.

92. Rosa PA, Tilly K, Stewart PE. The burgeoning molecular genetics of the Lyme disease spirochaete. Nature Reviews Microbiology. 2005;3(2):129-43.

93. Syed KA, Klose KE. *Vibrio cholerae* flagellar synthesis and virulence. In: Epidemiological and Molecular Aspects on Cholera. Springer; 2011. p. 203-12.

94. Correa NE, Peng F, Klose KE. Roles of the regulatory proteins FlhF and FlhG in the *Vibrio cholerae* flagellar transcription hierarchy. J Bacteriol. 2005;187(18):6324-32.

95. Kusumoto A, Shinohara A, Terashima H, Kojima S, Yakushi T, Homma M. Collaboration of FlhF and FlhG to regulate polar-flagella number and localization in vibrio alginolyticus. Microbiology. 2008;154(5):1390-9.

96. Balaban M, Joslin SN, Hendrixson DR. FlhF and its GTPase activity are required for distinct processes in flagellar gene regulation and biosynthesis in *Campylobacter jejuni* . J Bacteriol. 2009;191(21):6602-11.

97. *E. coli* chemotaxis [Internet]. Utah: University of Utah Department of Biology Parkinson Lab; 2012 [updated October 22, 2012; cited Jan. 12, 2013]. Available from: http://chemotaxis.biology.utah.edu/Parkinson_Lab/projects/ecolichemotaxis/ecolichemotaxis.html.

98. Wadhams GH, Armitage JP. Making sense of it all: Bacterial chemotaxis. Nature Reviews Molecular Cell Biology. 2004;5(12):1024-37.